X-ray Microcalorimeter Technology Roadmap

Table of Contents

This document presents a roadmap for advancing the critical technology of the *Lynx* X-ray Microcalorimeter (LXM). This technology roadmap describes the LXM elements that need to be developed, identifies the maturation plan key milestones, and details the associated schedule, cost, and risk. LXM is one of three science instruments required for the *Lynx* mission, and will provide high-spectral resolution, high-spatial resolution non-dispersive imaging spectroscopy over a broad energy range (0.2 to 10 keV). At the heart of LXM are arrays of low-temperature detectors, chosen because they are the only known method suitable for enabling such capabilities in this bandpass.

1 Introduction

The *Lynx* X-ray Microcalorimeter (LXM) is a broadband, non-dispersive, high-spectral resolution imaging spectrometer that consists of a large array of X-ray sensors that, when cooled to 50 mK, determine the precise energy. The predecessors to LXM are microcalorimeter spectrometers such as the Resolve instrument on the *X-ray Imaging and Spectroscopy Mission* (*XRISM*) (a rebuild of the Soft X-ray Spectrometer on *Astro-H*) launching in 2022, and the X-ray Integral Field Unit (X-IFU) on *Athena*, scheduled to launch in 2031. Resolve has 36 pixels and X-IFU has 3,168 pixels, whereas the LXM instrument concept consists of just over 100,000 pixels, with three pixel types (each optimized for different energy ranges) and pixel pitches several times smaller than on previous instruments. The specific LXM detector array architecture, described in Fig. 1, is key to achieving the three *Lynx* science pillars by not only providing high-resolution imaging spectroscopy, but with spatial resolution far exceeding that of previous microcalorimeter missions.

The LXM technologies are separated into four main elements, listed in Table 1 (for a detailed list of subelements, see Table 3). All elements are assessed at Technology Readiness Level 3 (TRL 3) or higher, with all expected to reach TRL 4 by 2021 with considerable schedule margin; it is more likely that TRL 4 will be achieved by the end of calendar year 2019 under existing NASA programs.

Table 1—LXM techology elements and current TRLs.

E#	LXM Element Description	Current TRL	Note
1	Large format, high spectral resolution microcalorimeter Pixel Arrays	3	Should reach TRL 4 in CY19
2	Microcalorimeter Readout	3	Should reach TRL 4 in CY19
3	Focal Plane Assembly and filters	4	
4	Cryogenics	4	

There has been significant technology investment and development, which has led to a number of recent breakthroughs that has fueled rapid TRL advancement, making the LXM concept feasible. Three major breakthroughs are listed below. Items (1) and (2) combined make Element 1 very close to TRL 4, and (3) makes Element 2 close to TRL 4, despite the over 30× increase in number of pixels in the focal plane compared to *Athena*'s X-IFU.

1. The successful demonstration of a type of microcalorimeter in which many pixels are attached to a single temperature sensor, called *hydras*. *The LXM consists of hydras with as many as 25 pixels attached to a single sensor.*
2. The integration of microcalorimeter arrays with fine-pitch, multilayer, superconducting wiring buried beneath a planarized substrate. *This advance was made possible by leveraging*

over a decade of investment in infrastructure and process development for superconducting digital electronics and quantum computing. The production of this type of wiring, critical to fine-pitch, large-format arrays, is now routine, and *allows fabrication of the required array size with high yield (~100%) and reliability.*

3. The development of a new type of microcalorimeter readout that uses Superconducting Quantum Interference Devices (SQUIDs) coupled to microwave resonators. *This readout technique has dramatically advanced the number of sensors read out on each signal chain*, from the range of tens (for the X-IFU) to hundreds. *This has leveraged readout technology developed for infrared detectors and, in particular, the approach pioneered for the development of microwave kinetic inductance detectors (MKIDs).*

Recent advances have been so successful that fully wired microcalorimeter arrays, with over 55,000 microcalorimeter pixels (spread over the three different pixel types needed for LXM), have been fabricated. Results from large prototype arrays using Transition-Edge Sensors (TESs) have shown that the performance requirements for all pixel types are feasible. A full-size LXM microcalorimeter array is under development, with fabrication scheduled to be completed in late 2019.

Based upon these advances, a subgroup of the *Lynx* Instrument Working Group comprised of 16 scientists and engineers who represent leading developers and innovators in the area of X-ray microcalorimetry developed the LXM instrument concept over the past three years. The instrument design meets the science requirements for a number of ground-breaking new observations while minimizing the resources and complexity to make it as practical as possible. The detailed design is described in a series of seven articles published in a special edition of the *Journal of Astronomical Telescopes, Instruments, and Systems* (*JATIS*) [Bandler et al. 2019, Bennett et al. 2019, Dipirro et al. 2019, Eckart et al. 2019, Sakai et al. 2019, Smith et al. 2019, Stevenson et al. 2019]. All of the groups envisioned to work on the development described in this roadmap have funded programs with the specific goal of LXM TRL advancement, or have plans to begin this work in the near future. The groups in the best position to produce the detectors and readout are already funded through NASA's Astrophysics Research and Analysis (APRA), Strategic Astrophysics Technology (SAT), and Internal Scientist Funding Model (ISFM) programs.

This technology roadmap is a planning tool that lays out the steps, activities, and resources needed to develop the LXM from the current State of the Art (SOA) to TRL 5 by project Phase A and to TRL 6 by Preliminary Design Review (PDR), ensuring that the instrument meets the scientific and programmatic requirements of the *Lynx* Observatory. Although TES-based X-ray microcalorimeters can be considered TRL 5 based upon the status of arrays developed for the *Athena* X-IFU and major advances relevant to the LXM design have been demonstrated, here an overall instrument TRL of 3 has been assigned, representing the lowest TRL of all critical technologies. Technologies for LXM were assessed at TRL 3 in the 2017 Physics of the Cosmos Program Annual Technology Report; however, the majority of the instrument is now at TRL 4, and some components even higher. The recent major advances (listed above) lend confidence to the notion that advancement of key components to TRL 4 and system-level demonstrations to TRL 5 are straightforward.

There are many details associated with demonstrating technical readiness of this complex instrument, just as there are for Resolve and X-IFU. This roadmap includes many of these details, in large part because we know so much about the approach we intend to pursue. This document also provides the technology maturation schedule, cost, risks, and mitigation plans. The LXM technology roadmap is a living document and will be updated as progress is made, or conditions affecting the plan become known.

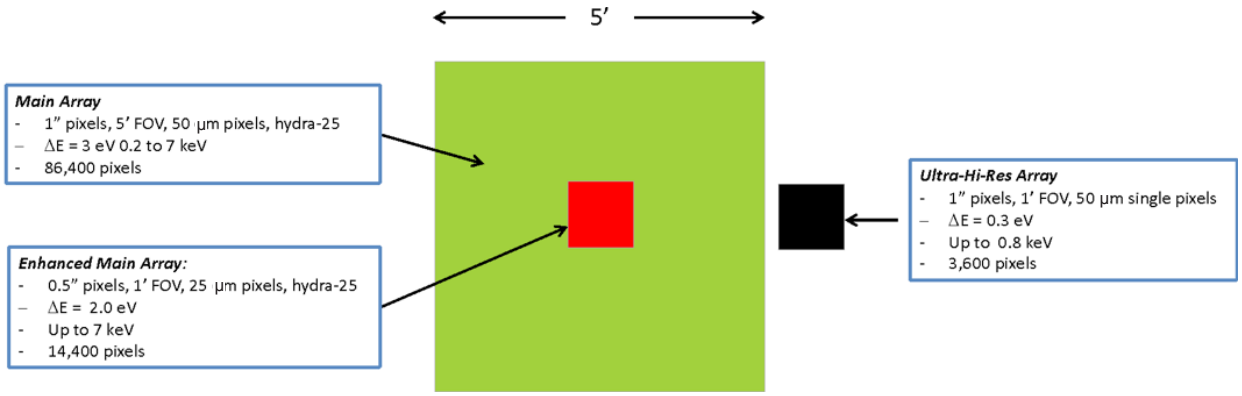

Fig. 1—This image shows the baseline layout of the LXM focal plane array. It consists of three different styles of pixels in three different regions. The Main Array consists of 1-arcsecond pixels over a 5-arcminute field of view with a 7-keV energy range. The Enhanced Main Array possesses 0.5-arcsecond pixels in the innermost central 1-arcminute region. Off to one side is the Ultra-Hi-Res Array consisting of 1-arcsecond pixels over a separate 1-arcminute region, optimized for high-energy resolution below 1 keV.

1.1 LXM Overview

The LXM is composed of a large array of X-ray sensors that determine the energy of individual incident photons by precisely measuring the temperature rise from the heat deposited. It will meet the many different science-driven performance requirements of *Lynx* with different subregions of the detector array. These arrays are identified as the Main Array (MA), the Enhanced Main Array (EMA), and the Ultra-High-Resolution Array (UHRA), and are described in Fig. 1. Each array is optimized for different combinations of spatial and spectral resolutions, energy ranges, count rate capabilities, and Fields of View (FOVs). The driving requirements for each of the three subarrays and the main science drivers for them are summarized in Table 2 (from the Science Traceability Matrix). More detailed requirements are available in the LXM overview article [Bandler et al., 2019].

Table 2—LXM mapping to *Lynx* science goals and drivers.

Main Array	Requirement	Science Drivers
Energy Range	0.2–7 keV for 3 eV	Low temperature (<1 keV) thermal emission or low energy non-thermal sources
Field of view	5 arcmin x 5 arcmin	Encompasses full supernova remnant (SNRs), galaxies, and clusters of galaxies for high-res imaging and spectroscopy
Pixel size	1 arcsec x 1 arcsec	Arcsecond scale features in shocks and filaments, and point sources in crowded regions (X-Ray Binary (XRBs) and stars)
Energy Resolution	3 eV (FWHM)	Map the structure of stellar-driven winds in galaxies (typical velocities 100–1,000 km/s)
Enhanced Main Array	**Requirement**	**Science Drivers**
Energy Range	0.2–7 keV for 3 eV	Low temperature thermal emission or low energy non-thermal sources
Field of View	1 arcmin x 1 arcmin	Jets, centers of galaxies, and cores of clusters of galaxies
Pixel Size	0.5 arcsec x 0.5 arcsec	Sub-arcsecond features in shocks and filaments, and point sources in crowded regions (XRBs and stars); study of distribution of AGN within and around groups/clusters; removing AGN; study of thermodynamic properties of cluster gas; feedback in groups and clusters
Energy Resolution	2 eV (FWHM)	Energetics and dynamics of plasmas, Supermassive Black Hole growth (resolving Fe K line profiles), Active Galactic Nuclei (AGN) feedback at peak (typical velocities ~100 km/s), and temperature and velocity profiles within the Bondi radius for a sample of Supermassive Black Holes

Ultra-Hi-Res. Array	Requirement	Science Drivers
Energy Range	0.2–0.75 keV	Faint diffuse baryons in emission, such as in galactic halos
Field of View	1 arcmin x 1 arcmin	Sample hot gas around galaxy halos
Pixel size	1 arcsec x 1 arcsec	Arcsecond-scale features in shocks and filaments, and point sources in crowded regions (XRBs and stars)
Energy Resolution	0.3eV (FWHM)	Velocities/turbulent broadening down to ~50 km/s (outflows and thermal velocities)

1.2 LXM Description

1.2.1 Detectors

There are a number of candidate thermal-sensor technologies, with the leading two for *Lynx* being microcalorimeters based upon TESs [Irwin and Hilton 2005] and Metallic Magnetic Calorimeters (MMCs) [Fleischmann et al. 2005]. These thermometer technologies both utilize the same multiplexed readout technology, incorporating SQUIDs in resonator circuits with resonance frequencies in the GHz range [Mates et al. 2017]. A single-pixel TES design is depicted in Fig. 2(a), and MMC design is shown in Fig. 3. For these devices, the energy resolution is determined by the accuracy with which a very sensitive thermistor can measure a temperature rise on a background of temperature fluctuations caused by the random transport of energy between a body with heat capacity C and the temperature bath to which its connected by a thermal conductance G. This is what is commonly known as thermodynamic noise, which scales as $T\sqrt{C}$, where T is the temperature and C is the microcalorimeter heat capacity. For high energy resolution, low temperatures (<0.1 K) are needed to minimize C and these fluctuations, so the devices are cooled to 50 mK. TESs and MMCs have the greatest potential of meeting LXM requirements, and recently have been under development specifically for the LXM. An important device architecture suitable for LXM is one in which multiple pixels are read out using the same sensor, commonly called hydras [Smith et al., 2019]. Hydras allow for some degree of thermal multiplexing to reduce the number of sensors that need to be read out, as shown in Fig. 2(b). In a hydra, a single sensor is attached to a number of different pixels (absorbers) via different strength thermal connections. The differences among pulse shapes before equilibration are used to determine the pixel that absorbed the X-ray photon. This multiplexing allows for finer sampling of the FOV compared with, for example, *Athena*'s X-IFU, without a commensurate increase in the number of wires, contacts, and readout components, or can be viewed as a way to increase the number of pixels by more than an order of magnitude without the commensurate increase in readout complexity.

Lynx has baselined microcalorimeters with TES thermometers for the LXM detectors because of the relatively high maturity level compared to MMCs and other thermometer technologies, although MMCs have some major potential advantages over TESs. Either TESs or MMCs will be selected for TRL 6 development.

As will be described in the next section on the SOA, both TES and MMC technology developments have already benefitted from the integration of high-density, multilayer wiring processes that are available from Massachusetts Institute of Technology's (MIT's) Lincoln Laboratory. They integrate buried superconducting microstrip wiring below the surface of the detector chips; thus, for the hydras, the buried wiring can be underneath the region occupied by the thermal links. This buried wiring process relies on chemical-mechanical polishing to planarize after each insulating layer to establish a pristine surface for subsequent depositions.

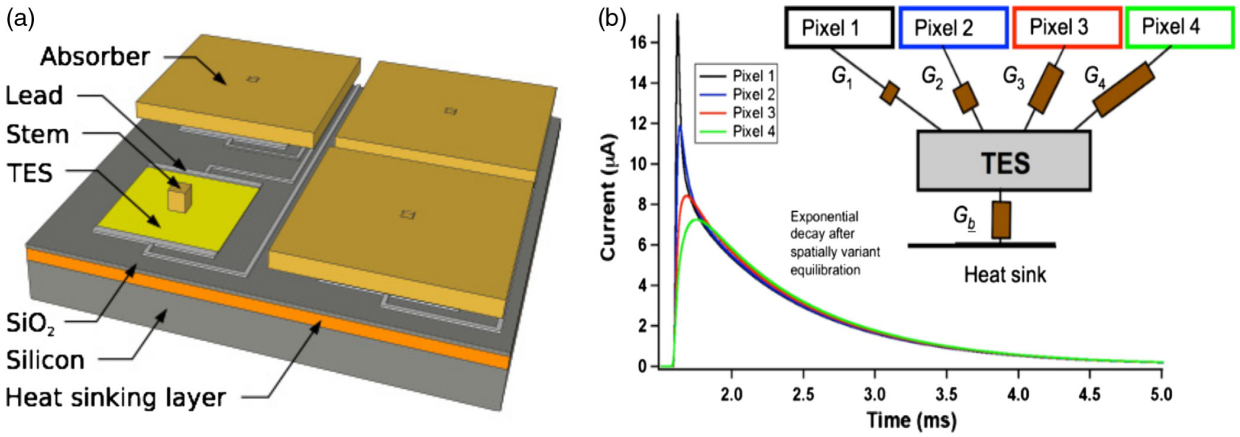

Fig. 2— (Left) Schematic showing components of a TES calorimeter. This design uses the thermal boundary between the TES film and the substrate for the necessary decoupling of the TES from the substrate. (Right) Schematic representation of the TES hydra. (Inset top right) Thermal model of a multi-pixel TES consisting of four X-ray absorbers connected to a single TES via varied thermal conductance G_i (where i = 1...4). The TES is weakly thermally coupled to a heatsink via conductance G_b. The measured average X-ray pulse shapes for a 4-pixel hydra at an energy of 6 keV are shown. The differences among pulse shapes before equilibration are used to determine the pixel that absorbed the X-ray photon.

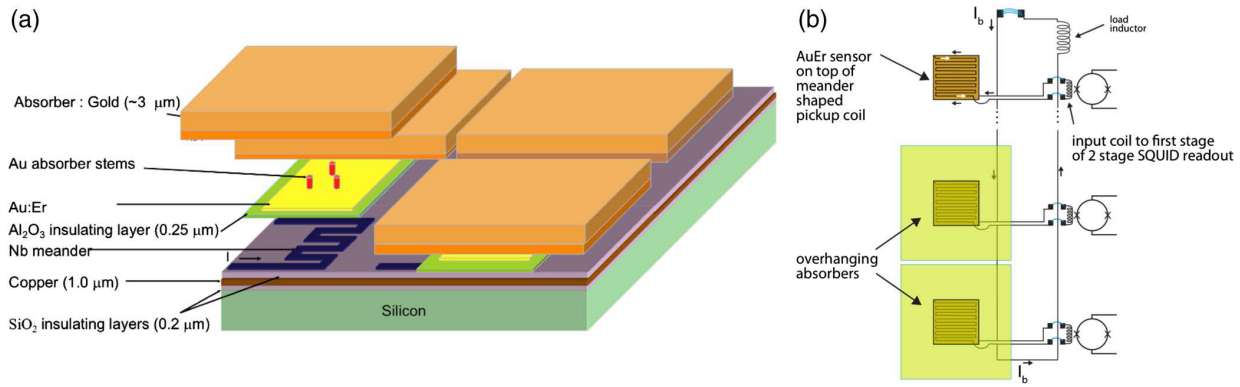

Fig. 3—(a) Components of a typical MMC design on a solid substrate. (b) Schematic for an array (only three shown) of magnetic calorimeter sensors. Each meander shaped pickup coil is directly coupled to the input coil of a current sensing SQUID. A common bias current is applied to all sensors.

1.2.2 Readout

The LXM TES (or MMC) arrays can be read out using microwave SQUIDs coupled to resonators that allow the multiplexed readout of hundreds of sensors on a single electronics chain. In a microwave SQUID multiplexed readout, the current signals from sensors biased with DC voltage stimulate RF-SQUIDs that change the effective length of microwave resonators coupled to a common feedline [Mates et al. 2017]. Fig. 4(a) shows a circuit diagram demonstrating how the sensors are inductively coupled to RF-SQUIDs, which in turn are coupled to the resonators, which are then capacitively coupled to the microwave feedline. A comb of microwave tones probe the resonators, and a shared semiconductor amplifier (e.g. a High-Electron Mobility Rransistor (HEMT) or a Silicon-Germanium Heterojunction Bipolar Transistor (SiGe HBT)) measures the summed tones. Typically, the tones are in the GHz regime, with the frequency spacing between tones set by the bandwidth requirements of the sensors. Microwave SQUID readout is advancing rapidly, with a recent 128-sensor-per-

microwave channel demonstration [Mates et al. 2017]. Bennett et al. 2019 reviews the current SOA for microwave SQUID multiplexing, describes how a microwave SQUID multiplexer can be optimized to meet the requirements for the different detector arrays proposed for the LXM, and describes the steps taken to advance the TRL of microwave SQUID multiplexing.

In addition, there is a backup readout technology—Code-Division Multiplexing (CDM)—that could read out the LXM TES arrays, but at a lower multiplexing factor. CDM uses a set of orthogonal modulation functions (Walsh codes) in which, during each time step, the signals from all TESs are summed with equal weight but different polarity patterns. In flux-summed CDM, the current signals from N microcalorimeters are passively summed in N-different SQUIDs with different coupling polarities [Irwin et al., 2010]. The signals from the SQUIDs are measured sequentially, as in a Time-Division Multiplexing (TDM) SQUID multiplexer. There has been a demonstration of the 32-channel CDM readout without significant energy resolution degradation on TESs [Morgan et al. 2016]. Additional detail on CDM is given in the next section. As in the case of the detectors, the readout technology (baseline or backup) will be selected for TRL 6 development.

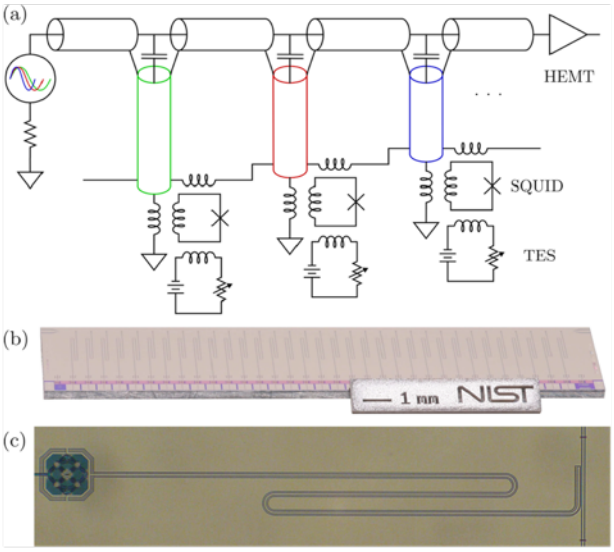

Fig. 4—(a) Diagram showing three channels of microwave SQUID readout circuit with TESs. (b) Photograph showing 33-channel microwave SQUID multiplexer chip. (c) Close-up photograph showing a quarter-wave microwave resonator capacitively coupled to a feedline. The resonator is terminated by an inductively coupled RF-SQUID [Mates et al. 2017].

1.2.3 Focal Plane Assembly and Infrared/Optical Blocking Filters

The preliminary Focal Plane Assembly (FPA) and blocking filters design for the LXM are shown in Fig. 5. Because the LXM FPA is similar in size to the *Athena* X-IFU FPA, it assumes leveraging much of the same technology in the mechanical design, thermal design, magnetic shielding, and design of the anticoincidence detector. (Because the anticoincidence detector will not require technology development, it is only addressed in this roadmap with respect to its incorporation into the FPA, not in the primary detector sections.) One of the key differences is the higher heat loads estimated for the LXM at 50 mK, and the associated higher cooling capacity Adiabatic Demagnetization Refrigerator (ADR). This difference allows the use of a mechanical support of the 50-mK stage that uses fiberglass thrust tubes to support the 50-mK stage from the 0.6-K stage and the 0.6-K stage from the 4.5-K stage, instead of the more traditional approach of using low thermal conductivity Kevlar strings for lower cooling power ADRs. These are shown on the left-hand side of Fig. 5. The use of these canonical thrust tubes and the accompanying thermal and structural performance will need to be verified in pre-Phase A and Phase A.

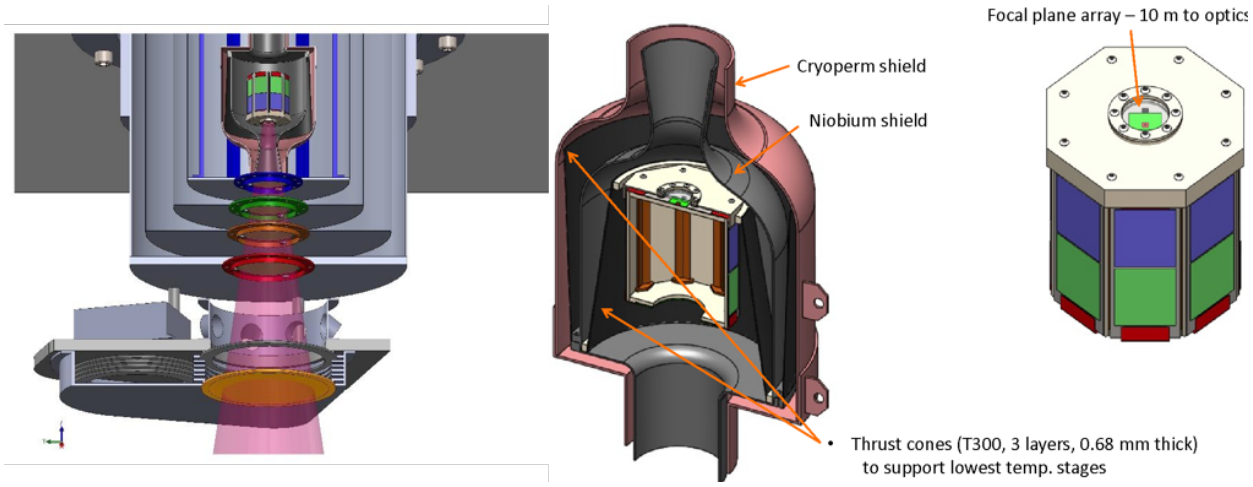

Fig. 5—Preliminary LXM focal plane assembly design and filter stack. (Left) Dewar model cross section highlighting the LXM filter mounting scheme. The dewar gate valve (door) is not shown. (Center) Cross-section of the FPA. The high-magnetic-permeability Cryoperm shield is at 4.5 Kevin and the superconducting niobium shield is at 0.6 Kelvin. (Right) Angled view of the FPA 50 mK stage. The Main, Enhanced Main, and Ultra High-Resolution Arrays are visible on the top surface through an infrared blocking filter that is transparent in this figure. The multiplexer readout components are on each of the 8 side panels.

1.2.4 Cooling System

The LXM will be cooled to 50 mK using a cryostat that takes advantage of the heritage of the flight-proven *Astro-H*/*Hitomi* ADR technologies. A detailed description of the cooling options under consideration for the LXM is given in [DiPirro et al., 2019]. The preliminary design for the cooling system is shown in Fig. 6. The key components in the cooling system are the cryocooler, which cools from room temperature (assumed to be 283 K in the thermal design) to 4.5 K, and then a multi-stage ADR that provides continuous cooling to 50 mK. The full complement of readout electronics is also shown in Fig. 6. The dominant heat loads from the detection chain at 4.5 K come from the HEMT amplifiers, estimated to dissipate 16 mW, and the harnesses, estimated to conduct 3 mW.

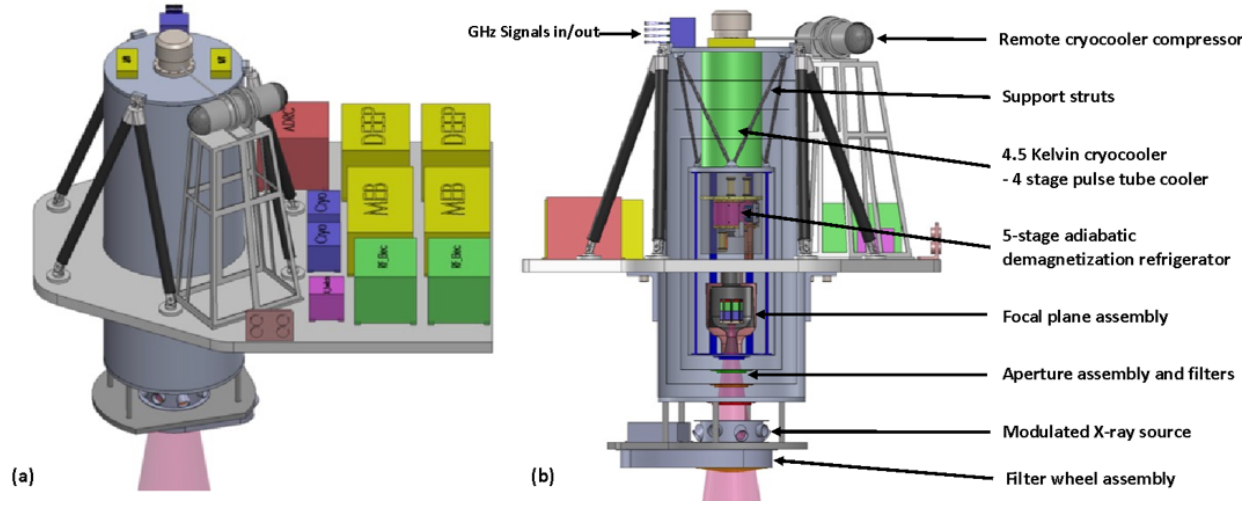

Fig. 6—(a) Overview of the LXM cryostat and readout electronics. (b) Side-on view of the LXM including a cross-sectional view of the cryostat. The X-rays enter the cryostat from the bottom. The filter wheel and modulated X-ray sources (with electronics) are located a small distance below the bottom of the main cryostat on a separate mounting plate, which is attached to the main cryostat. The height of the main cryostat shown is 1.43 m and the diameter is 60 cm.

There are a number of different options for providing 4.5-K cooling, but the preliminary design has been based upon the use of Advanced Cryocooler Development Program (ACTDP) 4-stage (Mega4-1) pulse tube cryocooler, of the type that is developed by Lockheed Martin. A Turbo-Brayton Cryocooler is also being considered for the 4.5 K cooling of the type that is developed by Creare.

1.2.5 Adiabatic Demagnetization Refrigerator

The LXM ADR provides continuous cooling at 0.6 K and 50 mK using a 5-stage ADR, as shown in Fig. 7. The design of this ADR and its controller are based upon the 3-stage ADR used for *Hitomi*. The continuous ADR is currently in development at NASA Goddard Space Flight Center (GSFC). The heat loads from the detection chain, thermometry dissipation, harness conduction, and suspension system, are estimated to be 124 μW at 0.6 K and 3.0 μW at 50 mK. The ADR is designed to meet these cooling requirements continuously with 100% margin, in accordance with NASA guidelines for cryogenic cooling margins. More details on the design of this ADR are described in [DiPirro et al, 2019]. A preliminary drawing showing how it is incorporated into the LXM is shown in Fig. 6(b).

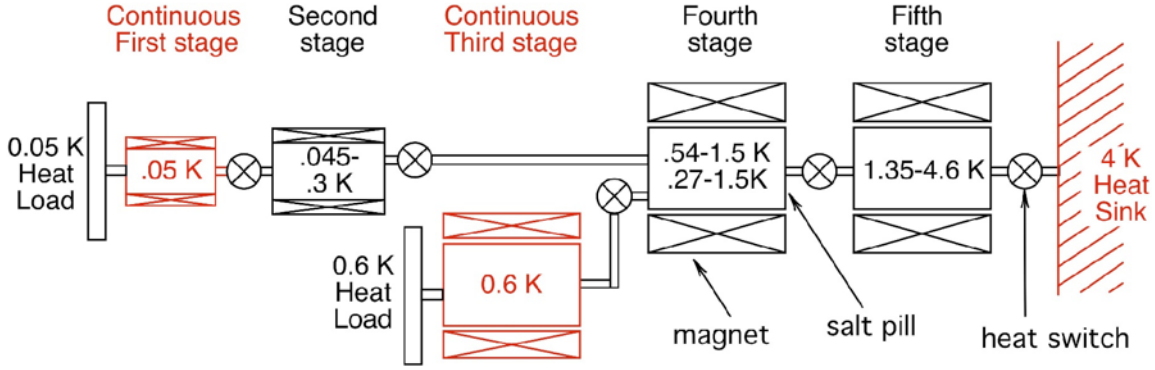

Fig. 7—The LXM multi-stage ADR design that produces the required cooling power at 50 mK and 0.6 K continuously, assuming a 4.5 K heatsink temperature. It consists of 5 different salt pills and 5 heat switches. Each salt pill is surrounded by its own magnet.

1.2.6 LXM Block Diagram

The block diagram for the complete LXM is shown in Fig. 8. This diagram shows all of the components of the LXM. It shows the two redundant electronics boxes for controlling the cryocooler and the redundant Main Electronics Boxes (MEB). Most of the electronics boxes consist of standard circuits and components used frequently for space, such as control microprocessors, conditioned power sources, and control signals for all of the various components and mechanisms. The Digital Electronics and Event Processor (DEEP) and the analog RF electronics boxes are the only ones that are technically demanding, and thus in need of technology development, as described in §1.2.2. Based upon our detailed master equipment list, our current best estimate for the mass is 468 kg. This is dominated by the mass of the cryostat (164 kg) and the mass of the electronics boxes (146 kg). Other significant contributions to the mass of the LXM come from the thermal system (72 kg), which is mainly the conventional heat pipes that connect the cryocooler and electronics boxes to the radiators.

The LXM technology development plan consists of research and development in four distinct areas, as well as in a number of subtopics within each area, as summarized in Table 3. The items that are reported at TRL 3 are close to TRL 4 based on recent advances.

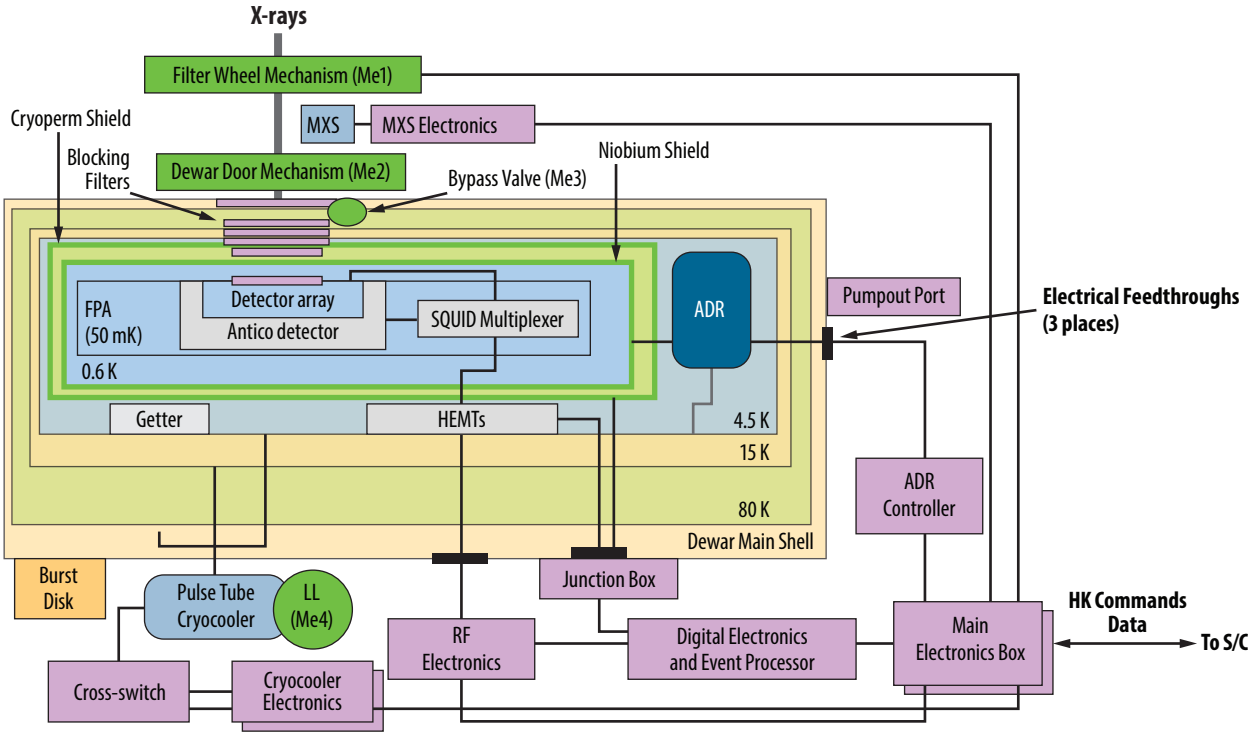

Fig. 8—LXM block diagram.

Table 3—Summary table of elements to be matured.

E#	Element Description	SOA Element TRL
1	Large format, high spectral resolution microcalorimeter pixel arrays	3
1.1	Microcalorimeter Arrays	3
1.2	Buried Superconducting Wiring	5
2	Microcalorimeter Readout	3
2.1	Microwave SQUID resonators	3
2.2	HEMT amplifiers	3
2.3	Readout electronics	3
3	Focal Plane Assembly and filters	4
3.1	Mechanical design and magnetic shielding	4
3.2	Interconnects	4
3.3	Bump-bonding	4
3.4	IR/Optical blocking filters	5
4	Cryogenics	4
4.1	Cryostat design	5
4.2	Cryocooler	4
4.3	Adiabatic demagnetization refrigerator	4

2 Detailed Technology Roadmap

In §2.1, Table 4 shows the LXM milestones for TRL 3. All LXM technology elements meet these TRL 3 criteria and the current SOA meets most (or all) of the TRL 4 milestones. Sections 2.2–2.5 describe in detail the SOA for each of the key LXM technologies. Section 2.6 presents tables summarizing the TRL 4, 5, and 6 milestones and the associated degrees of difficulty to achieve each level. Section 2.7 presents an in-depth discussion of each of the TRL 4, 5, and 6 milestones and the significance of each.

Table 4—LXM milestones for TRL 3.

NASA TRL Definition	Milestones for Achieving TRLs for the LXM
TRL 3 Analytical studies place the technology in an appropriate context and laboratory demonstrations; modeling and simulation validate analytical prediction.	Laboratory demonstrations of the key technologies which are the detector and the readout. For the detector, the operation of each of the three subarray pixel types should be demonstrated with form-factors (pixel size, pitch) and performance (energy resolution, energy range quantum efficiency) within a factor of 2 of what is needed to meet requirements. Specifically, they should meet the following characteristics and performance: • Multi-pixel detectors (hydras) demonstrated with absorber pitches <100 μm, with >10 absorbers attached to each sensor, demonstrating <5 eV energy resolution [FWHM] up to 6 keV (MA and EMA). • Single-pixel detector with pitch <100 μm demonstrating an energy resolution of <1 eV (FWHM) (Ultra-Hi-Res Array) at an energy of >0.5 keV. For the readout, the operational principle and basic performance of using microwave SQUIDs needs to be demonstrated with performance that agrees with expectation within a factor of 2. Specifically, a demonstration of the readout should meet the following characteristics and performance: • Representative readout architecture. • Degradation on intrinsic energy resolution of microcalorimeters (any type) less than a factor of 2 of what can be achieved with single-pixel readout. • At least 30 sensors read out simultaneously on a single readout channel. • Under the conditions of being in vacuum at realistic operating temperature and using laboratory electronics. **Model prediction**: Model predictions should show that: • Models of each of the three pixel types in the three subarrays can meet LXM performance requirements. • The electronics will be able to readout the pixel types with properties given by detector modelling of each of the three subarrays needed by the LXM, assuming a number of readout channels that are feasible within the cooling system and preliminary focal plane assembly designs. • A concept exists for wiring out all the pixels in the array using wire dimensions (pitches, thicknesses, gaps) previously demonstrated. • A concept exists for connecting all the wiring of detectors to the readout cold electronics, and then to the readout electronics at room temperature, using technologies that have previously been demonstrated. • Focal plane array design concept exists for housing the detector and cold readout electronics, with the required number of pixels. • A cooling concept exists using existing coolers or coolers modeled and currently in development that meets all the cooling requirements of the LXM at 4 K, 1 K, and 50 mK.

2.1 Description of Current State of the Art for Key Technologies

The LXM milestones for TRL 3 are shown in Table 4. The LXM technology elements have met all of these TRL 3 criteria.

2.2 Element 1 — Large Format, High Spectral Resolution Microcalorimeter Pixel Arrays

The LXM pixel layout includes multiple pixel array layouts. The basic design of the pixels for each of the array types are shown in Table 5.

Table 5—LXM arrays considered and their respective pixel design.

Tc = 65 mK	FOV	Type	Pixel Size	Absorber Thickness (μm)	DE (FWHM)	# of Pixels	# of Sensors	hydra (factor)	C (pJ/K)	G (pW/K)	Tau (ms)	Count Rate (cps)	TES Power (pW)	Shunt Power (pW)
Main Array	5'	25-pixel hydras	1"	4.0	3 eV	86,400	3,456	25	1.338	262	2.7	10.0	2.1	21
Enhanced Main Array	1'	25-pixel hydras	0.5"	4.0	2 eV	14,400	576	25	0.334	65	0.674	40.1	0.52	5.2
Ultra-Hi-Res Array	1'	Single pixel	1"	1.0	0.3 eV	3,600	3,600	1	0.013	22	0.324	83.3	0.173	1.73
Total						**104,400**	**7,632**							

2.2.1 State of the Art

The current X-ray microcalorimeter detector technologies required for LXM are presently evaluated at TRL 3, as described in Table 3. However, based upon progress in the development of small-pixel microcalorimeters over the past 10 years [Smith et al, 2012, Lee et al., 2015, Bandler et al., 2016, Smith et al., 2019, Bandler et al., 2019, and Smith et al, 2019 (2)], the TRL is now very close to TRL 4. A prototype LXM detector chip has been fabricated, with initial results indicating that it will meet the TRL 4 criteria for all array types.

There are two remaining milestones the TES-based approach needs to meet before reaching TRL 4:

1. Increase the energy range of prototype Ultra-Hi-Res Array measurements. This work is ongoing and expected to be completed in CY19.

2. Verify that the energy resolution and pixel discrimination properties (for the MA and EMA hydras) are maintained when measurements of existing devices are performed using suitable Nyquist inductors in the bias circuits. Such inductors are routinely added to slow down the pulse response (rise and fall), loosening the electrical dynamic range requirements of the readout multiplexer. Previous measurements on hydra pixels with suitable Nyquist inductors have shown no detrimental effects on the energy resolution and position discrimination [Smith et al, 2019], since the circuit filters the noise identically to the signal, and thus at most frequencies the signal-to-noise ratio is not degraded. These measurements must be reproduced on LXM-compatible hydras to reach TRL 4. Although this demonstration is an important step for determining the readout requirements, it is straightforward and should be completed in the next few months.

The development from TRL 4 to 5 is expected to be straightforward as well. TRL 5 calls for engineering work in scaling the prototype arrays to full-sized LXM arrays; however, the scale of arrays currently under test are already close to full sized.

There are two types of microcalorimeter detectors under development for LXM that are being developed in parallel by two different teams in order to reduce risk and determine which has the greatest potential for meeting the instrument requirements and goals. These are TESs [Smith et al., 2019, Bandler et al., 2019] and MMCs [Stevenson et al., 2019]. Both single-pixel devices and

multi-pixel devices (hydras) are under development with both TES and MMC sensor technologies. MMCs have some advantages over TESs, but MMCs are presently at lower TRL compared to TESs [Bandler et al, 2019]. MMCs have the potential for better intrinsic resolution than TESs, they are non-dissipative (so have a simpler thermal design), and have an intrinsically linear response to X-rays over a wide range of energies that can make calibration easier. However, the disadvantage of MMCs is that in order to take advantage of their better intrinsic resolution, an amplifier chain with lower noise is required. Thus, the parallel development of both TES and MMC arrays for LXM are complementary and helps to reduce the overall risk in the technology development plan. One will be selected for TRL 6 development.

The feasibility of both single-pixel arrays and multi-pixel hydras for high-resolution X-ray detectors has been demonstrated in a variety of geometries over the past decade. A hydra consists of multiple X-ray absorbers with a different thermal conductance to a single readout sensor. Each conductance is tuned to provide a different characteristic pulse shape and enables position discrimination between events absorbed in the different pixels.

2.2.2 Transition-Edge Sensors (Baseline LXM Sensor Technology)

The first LXM prototype arrays have been designed, fabricated, and tested, and initial indications are that they meet TRL 4 criteria. These new arrays are being developed by GSFC in collaboration with MIT's Lincoln Laboratory. Arrays have been fabricated that include all three subarray pixel types defined in Table 5. A prototype is shown in Fig. 9.

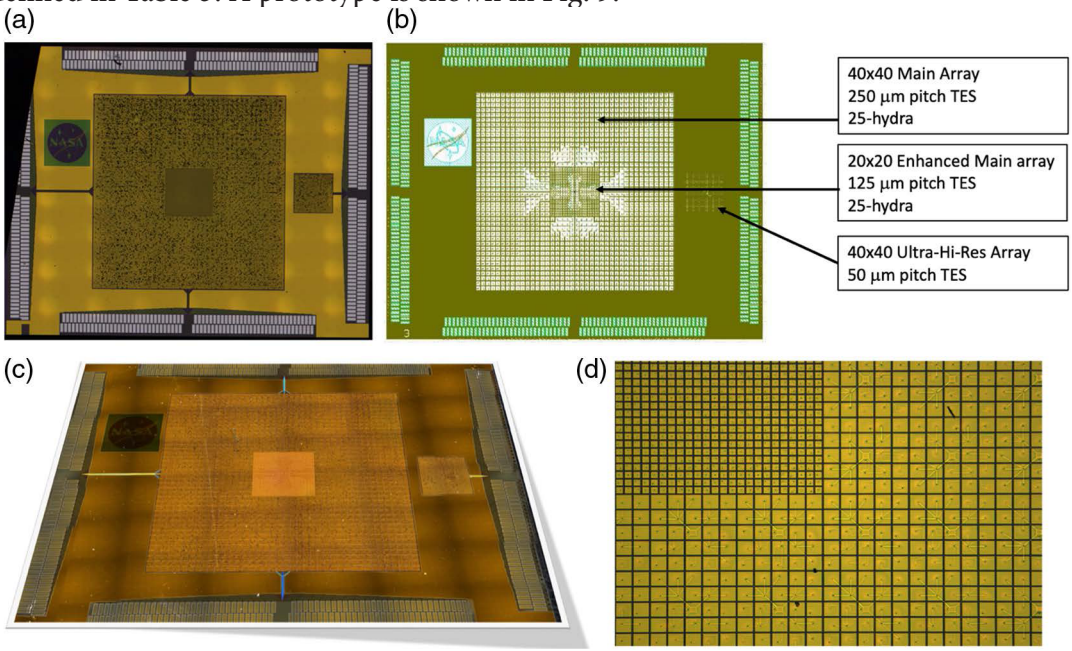

Fig. 9—Prototype LXM array. The dimensions of this chip are 1.9 × 1.5 cm. (a) Microscope image of a prototype array with nearly 50,000 pixels. (b) Mask layout showing different regions of the array and the internal wiring for a subset of the pixels. The labels show the regions and number and pitches of pixels for the three different subarrays. (c) Angled photograph of the array. (d) Zoomed-in view of a region of the array showing the interface between the Main Array and the Enhanced Main Array, highlighting the change in absorber pitch from 50 µm to 25 µm.

Following early proof-of-concept demonstrations described by [Smith et al. 2019], the MA and EMA hydra designs incorporate a hierarchical thermal link structure using trunks and branches that make it easier to design, lay out, and achieve uniform spacing of the absorber conductances. These LXM prototype chips also incorporate, for the first time, microstrip-buried wiring layers developed by Lincoln Laboratory that are of suitable pitch and density required to readout a full-scale LXM array.

LXM Prototype Array Results: Main Array — Tests have been carried out on a Main Array hydra with 50-μm pitch absorbers at X-ray energies of 1.5 keV and 6.4 keV, showing excellent results that are consistent with the TRL 4 milestones of $\Delta E_{FWHM} < 4$ eV at 6 keV, and with position discrimination down to 1.5 keV.

The measured energy resolution is $\Delta E_{FWHM} = 3.34 \pm 0.02$ eV for 1.5 keV Al-Kα X-rays (Fig. 10) and ΔE_{FWHM} ~3.3 eV±0.3 eV for 6.4-keV monochromatic x-rays. The average measured pulse shapes are shown in Fig. 10 (right); because of the hierarchical layout of the link structure, the pulse shapes have a complicated pre-equilibration signal.

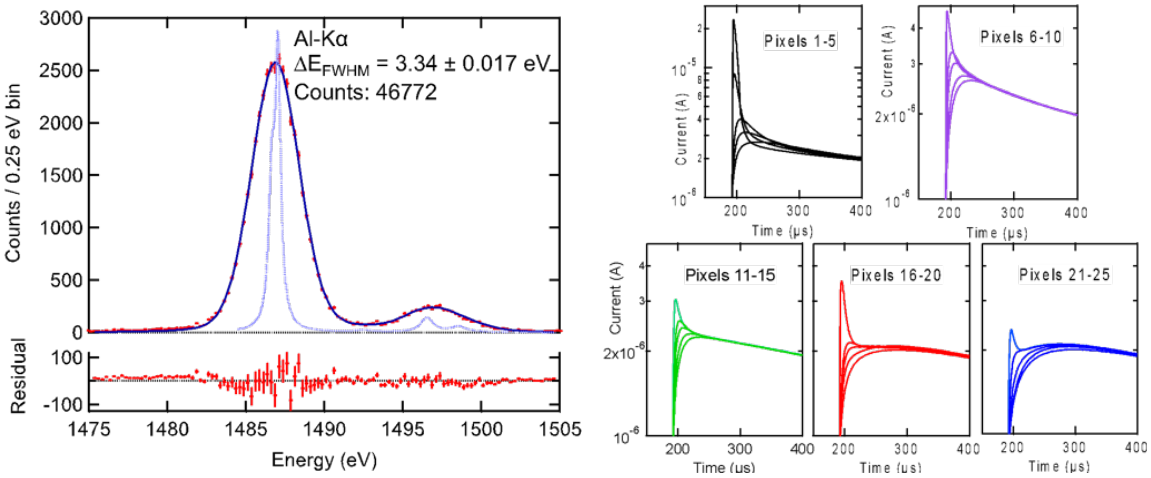

Fig. 10—(Left) Coadded Al-Kα energy histogram for all 25 pixels of a Main Array hydra. The best fit gives $\Delta E_{FWHM} = 3.34 \pm 0.02$ eV, and the average of the individually fitted histograms was $\langle \Delta E_{FWHM} \rangle = 3.37 \pm 0.31$ eV. (Right) Average measured pulse shapes for each of the 5 groups of pixels.

Both quoted resolution results are from the coadded energy spectra for all 25 pixels of a single hydra element. In the 1.5-keV measurement, the crosstalk noise is estimated to degrade the average resolution by ~20%, suggesting that ~3 eV is achievable with better heatsinking, as is planned for TRL 5. (The 6.4-keV result has a larger uncertainty due to a temporary problem with the data acquisition setup.) Previous measurements of a 20-pixel hydra at 5.4 keV [Smith et al. 2019] gave promising initial results, showing $\Delta E_{FWHM} = 3.39 \pm 0.18$ eV at 5.4 keV, albeit with 20% fewer pixels than a Main Array hydra. Measurements on these 20-pixel hydras also demonstrated that position discrimination was possible even at low energies, in this case verified for 277 eV C-Kα X-rays using a simple discrimination algorithm.

LXM Prototype Array Results: Enhanced Main Array — Tests have been carried out on an Enhanced Main Array hydra with 25-μm pitch absorbers at an X-ray energy of 1.5 keV. These results are consistent with the TRL 4 milestone of showing position discrimination down to 1.5 keV. The demonstrated energy resolution at 1.5 keV and preliminary measurements at 5.9 keV are consistent with the TRL 4 milestone of $\Delta E_{FWHM} < 3$ eV at 6 keV.

Fig. 11(left) shows the average measured pulse shapes for an Enhanced Main Array device at

1.5 keV (Al-Kα X-rays). The inset shows a zoom-in of the first 40 μs. Because of the hierarchical layout of the link structure, the rising edge of each pulse cannot be uniquely characterized by a single rise-time calculation, but a simple preliminary analysis already is sufficient to discriminate the 25 discrete populations of Al-Kα X-rays corresponding to each pixel in the hydra. For example, Fig. 11(right) shows a scatter plot of the rise-time calculated from the 10%–50% point of the pulse-height versus rise-time calculated from the 20%–80% point after smoothing the pulse to suppress the fast component. Various techniques are under study to extract position information from the pre-equilibration signal that are robust to the effects of pulse shape non-linearity with energy, and the tradeoff between processing power and effective discrimination will be examined, with principle component analysis being the most processing-heavy option studied.

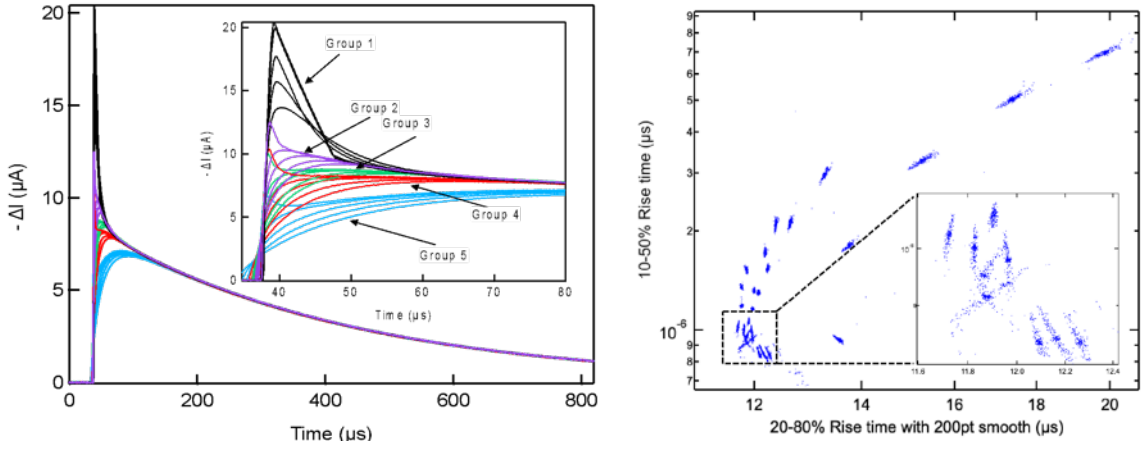

Fig. 11—(Left) Average Al-Kα pulse shapes for an EMA hydra. The inset shows a zoom-in of the first 40 μs, with the different groups of pixels identified. (Right) Rise-time scatter plot for an EMA hydra.

The energy resolution of this Enhanced Main Array device is excellent, as is the corresponding uniformity. Fig. 12 (left) shows the coadded energy histogram for all 25 pixels at Al-Kα with a fitted resolution $\Delta E_{FWHM} = 1.66 \pm 0.02$ eV, consistent with the average of all pixels fitted individually, $\langle \Delta E_{FWHM} \rangle = 1.68 \pm 0.13$ eV. Shown in Fig. 12 (right) is ΔE_{FWHM} from the individual energy histograms versus pixel number, illustrating a high degree of resolution uniformity. Shown for comparison is the resolution calculated from the integration over frequency of the Noise-Equivalent-Power, NEP(f),

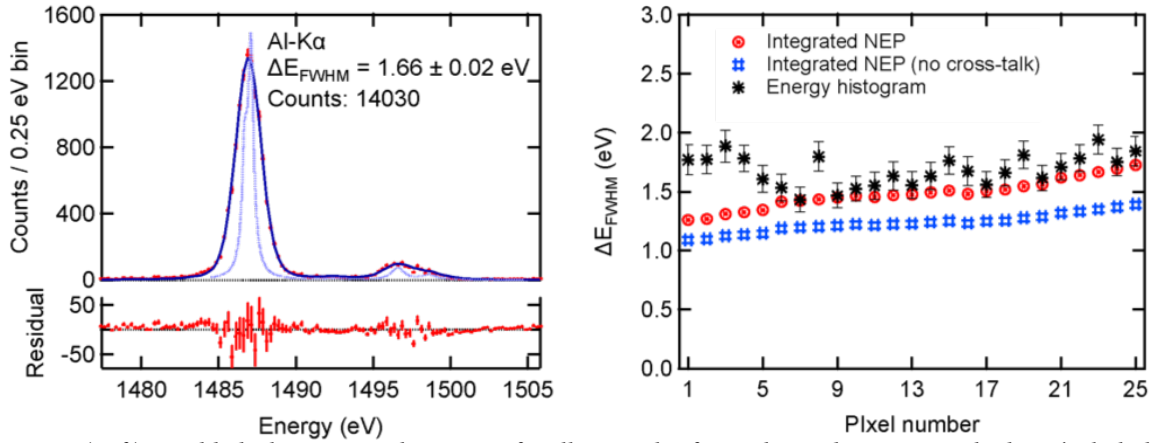

Fig. 12—(Left) Coadded Al-Kα energy histogram for all 25 pixels of an Enhanced Main Array hydra. The light blue line shows the intrinsic linewidth for Al-Kα. The dark blue line gives the best fit to the date, with an energy resolution of the hydra of $\langle \Delta E_{FWHM} \rangle = 1.66 \pm 0.02$ eV. (Right) ΔE_{FWHM} versus pixel number within the hydra, including that from individually fitted energy histograms (black stars), and the predicted resolution from the integrated NEP(f), measured both with (red circles) and without thermal crosstalk noise (blue boxes).

where NEP(f) is determined from measurements of the average pulse shape and noise spectral density. As expected, the integrated NEP(f) degrades slightly as the bandwidth of the pulse is reduced by the low-pass filtering from the links. By comparing the integrated NEP(f) calculated using noise measured with and without X-rays illuminating the array (shown on Fig. 12 (right)), it is estimated that thermal crosstalk noise degrades the resolution by about 20% at the measurement count-rate of ~1.5 ct/s/pixel. Thus, it is reasonable to assume that for future designs with optimized heatsinking layers, improved ΔE_{FWHM} will be achievable. High statistics measurements at Mn-Kα (5.9 keV) have not been taken; however, low statistic measurements showed the average of the integrated NEP(f), without the thermal crosstalk was 1.55 eV. This compares to 1.23 eV at Al-Kα and suggests that once the heatsinking has been incorporated, ΔE_{FWHM} should be close to meeting the 2-eV design goal for energies up to 7 keV (and far exceeding the TRL 4 milestone).

LXM Prototype Array Results: Ultra-Hi-Res Array — Testing of an Ultra-Hi-Res Array pixel has shown $\Delta E_{FWHM} = 0.26$ eV at a photon energy of 3 eV (Fig. 13), significantly better than the 0.5 eV required resolution of the TRL 4 milestone, and close to the required resolution for the UHRA, albeit only verified at the low-energy part of the bandpass. These devices had approximately 2× higher heat capacity than the original design goal, which suggests further resolution improvements may readily possible.

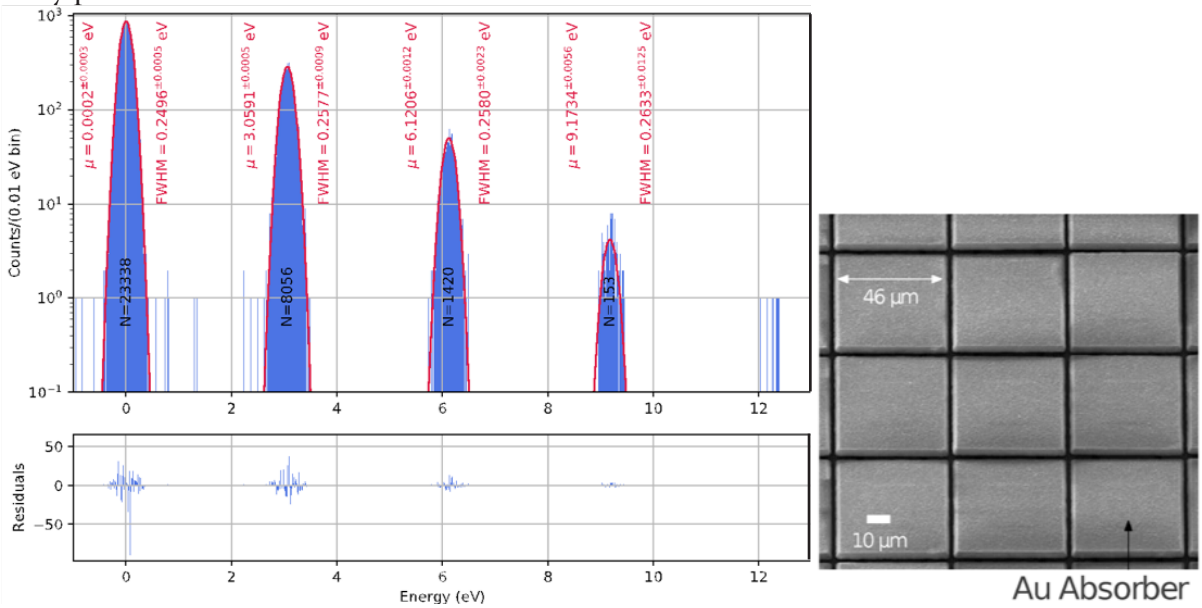

Fig. 13—(Left) Measured spectral resolution $\Delta E_{FWHM} = 0.26$ eV on an Ultra-Hi-Res Array TES pixel at a photon energy of ~3 eV, 6 eV, and 9 eV (corresponding to the absorption of 1, 2, and 3 of the 3.06-eV photons from a ultraviolet laser diode. (Right) Scanning electron microscope image of 9 pixels from a prototype UHR array.

These measurements were carried out using an Ultraviolet (UV) diode [Jaeckel et al., 2019] that can produce a comb of photon energies in multiples of 3.06 eV. In these initial measurements, the energy range was limited to ~9 eV, but future optimization of the experimental setup should allow measurements to >100 eV in the near-term and >500 eV within months.

Prior development of TES-based microcalorimeters (single pixels) with a 50-µm pitch provided excellent energy resolution at 1.5 keV, and were the basis of the development of the Ultra High Resolution Array pixel design. The previous results showed 0.72 eV at an energy of 1.5 keV [Lee et al. 2015], and analysis of the pixel suggested that better than 0.40 eV resolution was possible if properly

characterized using a more appropriate X-ray measurement source. These pixels had an Au absorber that was 4.2 μm thick, and it was straightforward to estimate that a similar TES pixel with an absorber of only 1–2 μm thickness could provide an energy resolution of 0.3 eV for energies below 1 keV.

2.2.3 Metallic Magnetic Calorimeters

Several key technology elements enabling an MMC option for LXM have been developed over the past two years. Sensor designs with sufficiently high inductance to mitigate stray wiring inductance expected in LXM array sizes have been completed, and fabrication of such devices has been demonstrated with submicron-pitch sensor coils, using deep-UV projection lithography. High-yield, high-critical current density fabrication of these sensors has been achieved using two-level buried wiring, similar to that used for the TES advances and also performed at MIT's Lincoln Laboratory. Full-scale LXM prototype arrays with high-inductance sensors and four-level buried wiring, as well as an innovative sensor topology and thermal design, are shown in Fig. 14. This prototype is similar in scale to the version developed for TESs.

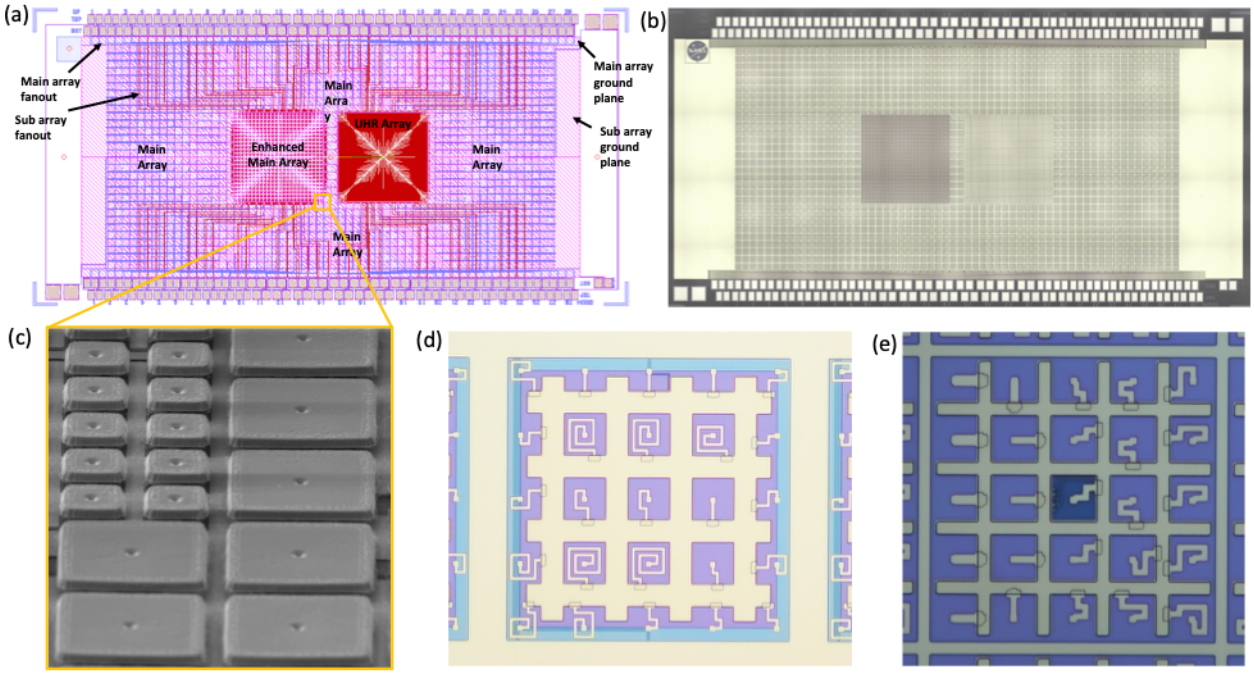

Fig. 14—Prototype LXM array using metallic magnetic calorimeters. (a) Design layout of the entire prototype array in which all of the pixels are wired within the array. The blue lines are the wiring to the Main Array, the purple lines are for the Enhanced Main Array, and the red lines are for the Ultra-Hi-Res Array. There are 112 bond pad pairs spread across two rows along both the top and bottom edges. (b) A completely fabricated prototype. (c) Scanning electron microscope image of a small region of the array that shows the interface between the Main Array pixels and the Enhanced Main Array pixels. The 2.8-μm-thick gold pixel absorbers are cantilevered above the substrate on small stems that make contact in the pixel centers. (d) Main Array hydra before the 25-pixel absorbers were added (pixels on a 50-μm pitch). The waffle-shaped region is the MMC sensor, and the lengths and widths of the lines between the waffle and central pixel stem locations determine the thermal conductance to each pixel. (e) Enhanced Main Array hydra before the 25 absorbers were attached, these pixels being on a 25-μm pitch.

This prototype chip is 2 × 1 cm and contains bond-pads for reading out a total of 112 sensors (single pixels and hydras). The layout is slightly different in approach to the TES LXM prototype. It consists of a basic envelope that is half of the LXM Main Array in scope, with 30 rows of MMC

sensors and 60 columns, with each sensor connected to 25 pixels in a hydra geometry. Within this envelope are full-size prototypes of the other two subarrays. There is a full-size Enhanced Main Array in the left central region, with 24-×-24 arrays of 25-pixel hydras. Then there is a full-size Ultra-Hi-Res Array 60-×-60 array with single 50-μm pixels per sensor. In total, there are 55.8 kilo-pixels in this array. What is particularly noteworthy is that every single pixel is wired from the pixels to the outside of the region of the array; this was achieved using an automated algorithm for laying out the positions of all the wires. It required the use of four different Nb layers, as opposed to the two layers used in the TES prototype. See [Stevenson et al. 2019] and [Devasia et al. 2019] for more details.

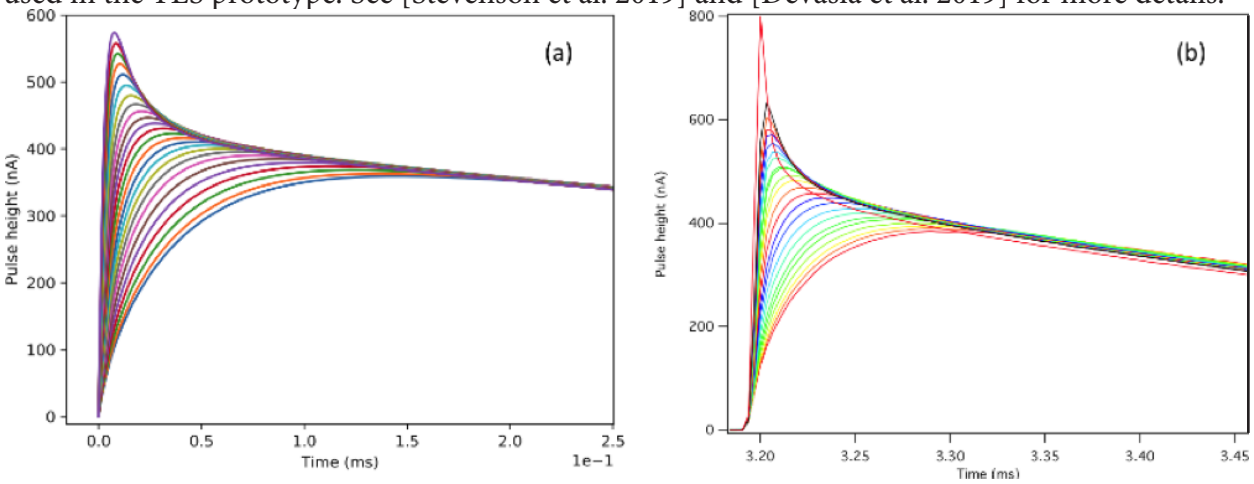

Fig. 15—Initial results from the LXM MMC prototype array. (a) Simulated and (b) measured pulse-shapes from an MMC hydra with 25 absorbers attached on a 50-μm pitch, from the MMC Main Array.

These first prototype arrays are still being tested, but the initial results are very encouraging. Fig. 15 shows the simulated and measured pulse-shapes from one hydra tested at 50 mK. Both the magnitudes and shapes of the measured pulses are clearly very similar to those from the model. For the responsivity measured so far, modeling predicts an energy resolution for the different pixels when coupled to a readout optimized for the properties of these sensors, as shown in Fig. 16. Thus, it appears that the MMC hydras fabricated are already capable of meeting the Main Array requirements (and indeed all the subarray requirements), and a lot of further optimization is still possible.

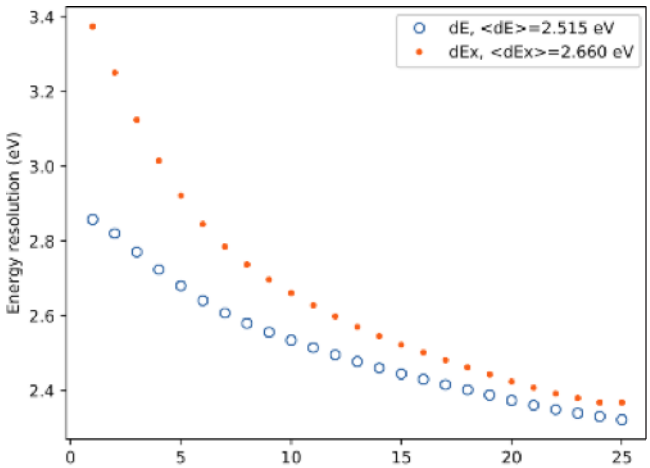

Fig. 16—Simulation predicting the FWHM energy resolution of the 25-pixel hydra sensor with 0.8 μm pitch meander coil in the MMC Main Array in LXM, operating at 40 mK. The energy resolution without errors in position correlation is dE, while dEx includes the effect of uncertainty in determining the X-ray absorption location for an X-ray energy of 200 eV. For X-ray energies much larger than 200 eV, the energy resolution approaches dE.

First tests of a hydra from the Main Array gave an estimated energy resolution based upon the signal shapes for MnKa X-rays at 5.9 keV and the observed noise, of 2.8–3.7 eV at 50 mK. This sensor was not yet coupled to an optimized readout, which would improve the energy resolution by a factor of 1.6. Further design optimizations that could lead to even better performance. Therefore, an energy resolution well below the required 3 eV seems

very achievable, but more development and tests are needed. Similarly, a pixel from an Enhanced Main Array prototype has been measured at 50 mK and demonstrated a predicted energy resolution based upon the signals and noise of 1.96–1.99 eV for the 26 different pixels of the hydra. These measurements were also not with an optimized readout design, which should improve the numbers by a factor of approximately 1.6; further updates to the design are possible. Also energy resolution well below the required 2.0 eV for this subarray appears to be possible. Therefore, MMCs appear to also have high potential for providing a parallel path towards producing the microcalorimeter array needed for the LXM.

2.2.4 Buried Wiring

Incorporating multiple layers of buried wiring utilizing a process that is already incredibly reliable and high yield will be a massive aid in helping the detector technologies advance more quickly to TRL 5. The wiring technology itself is already essentially TRL 5; however, there are further innovations important for both TESs and MMCs that involve the buried wiring that will need further development. The next iteration of these developments, described in the next paragraphs, are ongoing, and the next iteration will be fabricated within the next year from both the TES and MMC development programs.

In 2019, the use of additional MIT Lincoln Laboratory process capabilities will be used to introduce a buried heatsink layer underneath the buried multilayer wiring in order to reduce thermal crosstalk to an acceptably low level in TES arrays. This was previously demonstrated by [Finkbeiner et al., 2015]. This will involve the introduction of a silicon nitride layer and silicon oxide layer underneath the buried wiring. In parallel in 2019, the use of additional MIT Lincoln Laboratory process capabilities will be used to fabricate a full-scale fan-out of the buried wiring from the detector arrays (and subarrays) to indium bump-bond connections to 2D arrays of microwave SQUID multiplexers. This requires the stitching together of the central 2.1 cm^2 (with wiring widths down to 0.4 μm) to 4.84 cm^2 regions (which are the maximum reticle sizes currently available for the buried wiring with slightly wider wiring line-widths) to cover a large octagonal wafer ~8 cm across, large enough for the fan-out of all wiring in the array to the bump-bond contacts needed for both MMCs and TESs.

In the MMC prototype, the fan-out will make contact to readout chips through wire-bonds, as well as make the initial testing of the next devices simpler. DC and microwave connectivity of the superconducting fanout wiring using dummy models of resonator arrays will be demonstrated. In early 2020, MMC prototype arrays are expected to demonstrate hybridization of dummy resonator arrays to a detector wafer to show an FPA at full LXM size using an existing FC-150 flip-chip bonder at GSFC. In 2019, initial designs for integrated heat switches and coil designs will be incorporated that improve the performance of the MMC Ultra-High-Resolution Array prototypes to meet LXM requirements. Microwave SQUID technology advancements are also required, and a path to the necessary improvements in coupled energy sensitivity by use of higher inductance input transformers, lower noise parametric amplifiers, and higher flux ramp modulation frequency has been mapped out.

The TES array designs will also have every sensor wired out within the arrays (like the MMC arrays), and some novel TES designs incorporating a wiring level underneath the TES will also be tested. The first wafers with buried wiring yielding during the late summer, and the completely fabricated wafers around the end of the calendar year. In the future, more layers of wires will be utilized to provide greater electrical crosstalk mitigation, likely using layers of ground planes and layers providing coaxial-like shielding around the different signal wires.

2.3 Element 2 – Microcalorimeter Readout

2.3.1 State of the Art

The current TRL for the readout of our microcalorimeter arrays with microwave multiplexing is TRL 3, but, similar to the case of the LXM TES detectors, close to TRL 4. Based on published results of multiplexing demonstrations [Bennett et al. 2019 and references therein], microwave multiplexed readout of single-absorber TES microcalorimeters is TRL 4; however, the high slew rates required to match the pulse rise of the hydra microcalorimeters mean that microwave SQUID multiplexers will be specifically matched to each of the LXM pixel types [Bennett et al. 2019]. High-slew rate multiplexer demonstrations have been performed, providing experimental proof-of-concept for the needs of LXM, but, fabrication of the specific chips needed for an LXM TRL 4 demonstration has not (yet) been completed. Microwave multiplexing advances and demonstrations relevant to LXM are listed here.

There has been a demonstration of microwave readout of 128 TESs attached to microwave SQUID resonators on a single HEMT without energy resolution degradation from the readout [Mates et al. 2017] using a resonator bandwidth of 300 kHz and a channel at a spacing of 6 MHz. Using the same multiplexer design, [Yoon et al. 2018] have demonstrated simultaneous readout of five X-ray TESs achieving spectral resolutions between 2.8 eV and 3.1 eV FWHM at 5.9 keV, similar to the achieved resolution when this array was measured non-multiplexed. Additionally, similar multiplexers with resonators spaced by 3 MHz have been used in a demonstration that multiplexed 104 channels simultaneously [Bennett et al. 2019]. The combined X-ray spectrum of 82 of the channels achieved an FWHM energy resolution of 2.04 eV at 1.25 keV, consistent with the resolution achieved using standard time-domain multiplexing readout with the same detector array. Based on these demonstrations the TRL of microwave multiplexing of single TESs would be TRL 4.

A maximum slew rate of 3 A/s has been achieved in resonators with a 2-MHz bandwidth (and sample rate of 500 ks/s), which is consistent with spacing resonators by 14 MHz. The scaling of this slew rate with bandwidth was used to design the baseline *Lynx* readout for estimating the number of microwave readout channels (and thus HEMTs) needed for each array type listed in Table 6. A margin of 50% was maintained in the estimated slew rate capability compared to the required maximum (and thus integrated bandwidth of the readout), as shown in Table 6.

Table 6—Slew rate capability and maximum number of HEMTs for the different pixel arrays.

	Max Slew Rate (req.) (A/s)	Energy for this Slew Rate (keV)	Sample Rate (MHz)	Res. Width (MHz)	Res. Spacing (MHz)	# of Res. per HEMT	Slew Rate Margin (At 6 keV)	# of HEMTs	Round Up
Main Array	1.5	6	0.35	1.4	10	400	50%	8.6	10
Enhanced Main Array	6	6	1.4	5.6	40	100	50%	5.1	6
Ultra-Hi-Res Array	0.85	1	0.215	0.86	6	667	50%	5.4	6
Total							**Total coaxes**		44

Since the previous optimizations of microwave SQUID readout have been successful, the performance is well understood, and the necessary parameter space has already been experimentally proven, the advancement degree of difficulty is expected to be low. This particular set of desired design parameters has only relatively recently been established, and so there has not yet been sufficient time

to produce devices optimized for LXM and elevate the TRL accordingly. While we expect the TRL advancement to be rapid, there is significant margin in the LXM development schedule (see §2.8) that alleviates schedule risk if the optimization of this critical technology takes longer than anticipated.

The backup readout technology, CDM, uses a set of orthogonal modulation functions (Walsh codes), in which during each time step, the signals from all TESs are summed with equal weight but different polarity patterns. In flux-summed CDM, the current signals from N microcalorimeters are passively summed in N-different SQUIDs with different coupling polarities [Irwin et al. 2010]. The signals from the SQUIDs are measured sequentially as in a TDM SQUID multiplexer.

Flux-summed CDM requires each TES to be coupled to all SQUIDs within a column so leads must be lithographically routed from every TES to every SQUID. As the number of rows increases, the number of wire crossovers increases significantly, and eventually fabrication yield drops to the point that larger chips become impractical. With flux-summed CDM, it could be difficult to reach suitable yield at multiplexing factors of 48. One possible mitigation against multiplexer fabrication yield issues is to implement hybrid TDM/CDM. In the hybrid scheme, blocks of CDM are embedded in a larger TDM column, and each TES is coupled to more than one SQUID, but not to all SQUIDs within a column. Fig. 17 shows three ways to read out four TESs in one column: (1) standard TDM-4, (2) standard CDM-4, and (3) the hybrid scheme of CDM-2 X TDM-2, called CDM2xT2.

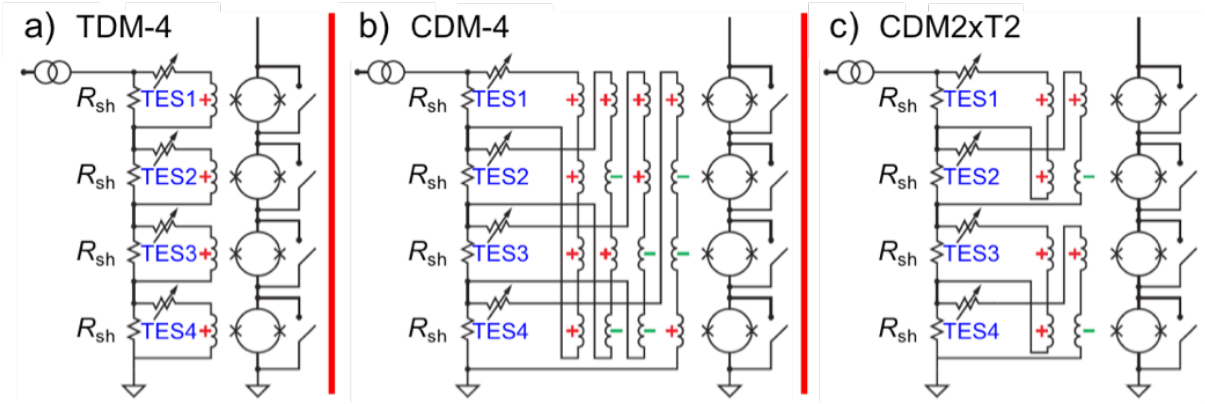

Fig. 17—Hybrid CDM. (a) Four-row TDM. (b) Four-row flux-summing CDM. (c) Hybrid: 2-row flux-summing CDM in time division with another 2-row flux-summing CDM, or CDM2xT2. In any of these three, the SQ1s are run as TDM-4. Only the TES couplings are different. The backup option is CDM16xT4, or four TDM'ed banks of CDM-16 each.

Microwave SQUID multiplexing requires readout electronics and focal plane architectures that are new to the microcalorimeter community. Although flux-summed CDM has not been demonstrated with hydra microcalorimeters, the maturity path is more straightforward since it is drop-in-compatible with TDM but also more capable than TDM. TDM currently has a TRL of 5 on non-hydra pixels, but is insufficient for reading out the number of hydras designed for the LXM when the slew rate requirements are considered. Flux-summed CDM can utilize the readout electronics, including the Goddard SpaceCube platform cards developed for TDM/CDM <https://spacecube.nasa.gov/>, and focal plane layouts, which have been demonstrated for TDM. CDM could have advantages in terms of power consumption and maturity; however, the lower multiplexing factor would add complexity to the focal plane. Also, the circuits are more complex, which makes it more difficult to achieve the required fabrication yield. The TRL of CDM for the readout of hydra microcalorimeters is currently TRL 3, but the advancement degree of difficulty should be low given the advanced state of the readout electronics.

Given the slew rate capabilities and current rate of progress in the development, the LXM

team expects that the microwave SQUID resonator readout approach will be the best match to LXM requirements. Hence, this approach is chosen as the baseline. CDM is an appropriate backup solution since it has different maturation risks than microwave SQUID multiplexing and builds on the previous development of TDM. A downselect will take place for TRL 6 development.

2.3.2 HEMT Amplifiers for Microwave SQUID Readout

State of the Art — HEMT amplifiers exist with input noise temperatures as low as 2.5 K over the 4- to 8-GHz band (Fig. 18). Several commercial vendors supply HEMT amplifiers. Various HEMT models cover lower and higher frequencies and narrower and broader bands with different noise temperatures. Commercial Low Noise Amplifiers (LNAs) exist that can provide gain after the HEMT stage. The 4-K amplifier continues to be referred to as the HEMT architecture even though, strictly speaking, there are several possible amplifiers. The architecture includes the number of stages, the thermal locations of the stages, and the gain, noise, power dissipation, and linearity of each stage. Linearity plays an important role in setting crosstalk levels. The connections between stages are important, and different types of connections are possible and suitable at different temperatures.

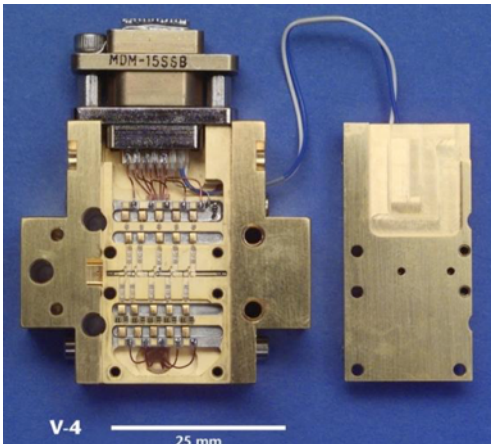

Fig. 18—HEMT amplifier fabricated by National Radio Astronomy Observatory (NRAO) for the Wilkinson Microwave Anisotropy Probe (WMAP) mission currently on display at the Smithsonian Air and Space Museum. Figure from <https://airandspace.si.edu/collection-objects/amplifier-wmap-cryogenic-inp-hemt-low-noise-amplifier>.

Readout Electronics — The room temperature electronics for the baseline readout uses microwave SQUID resonators in the 4- to 8-GHz range. These electronics mainly consist of Radio Frequency (RF) amplifiers, I/O mixers, and local oscillators (LOs), high-speed Analog-to-Digital converters (ADCs)/digital-to-analog converters (DACs), and Field Programmable Gate Arrays (FPGAs). In the laboratory, demonstrations currently read out 128 resonators with 500 MHz of bandwidth. These use Reconfigurable Open Architecture Computing Hardware (ROACH) electronics based upon commercially available Virtex®-6s, for which there is not currently a flight-compatible version. The LXM team has designed a flight-compatible readout that is capable of reading out the complete LXM array using flight-compatible ADCs, DACs, and FPGAs (UltraScale+™ MPSoC) that are either available today or will soon be available [Sakai et al. 2019]. The estimated power that is dissipated in the room temperature electronics is approximately 750 W.

The development of control electronics for microwave SQUID multiplexing (μMUX) will benefit from activities across the field of low-temperature detectors. Numerous U.S. research groups are exploring electronics solutions, including Arizona State, the Jet Propulsion Laboratory (JPL), the National Institute of Standards and Technology (NIST), GSFC, and SLAC. Furthermore, there is significant overlap between the functionality needed for μMUX control and the commercially active field of software-defined radio. As a result, the technology development can leverage commercial hardware and firmware activities. The technological risk of μMUX electronics development is mitigated by this combination of interest from research institutes and the private sector.

2.4 Element 3—Focal Plane Assembly and Filters

The microcalorimeter array, anticoincidence detector, and cold readout components are packaged inside an FPA. The FPA, at the instrument base temperature, provides thermal-mechanical isolation and electromagnetic shielding. The LXM will use a set of blocking filters mounted within the dewar that passes the X-rays of interest while attenuating the out-of-band, long-wavelength radiation that, if unfiltered, would degrade the performance of the microcalorimeters and cooling chain. The design of the LXM FPA is summarized in [Bandler et al. 2019] and the design of the LXM optical blocking filters is summarized in [Eckart et al. 2019].

2.4.1 State of the Art

Currently, FPA technologies with respect to the LXM FPA requirements are at TRL 4. The IR/optical blocking filters are at TRL 5. Backup technologies for the filters that could enhance the instrument throughput in the soft X-ray bandpass are at lower TRLs (~TRL 2/3).

2.4.2 Mechanical Design and Magnetic Shielding

Because the LXM FPA is similar in size to the *Athena*'s X-IFU FPA, the LXM will leverage much of the same technology in the mechanical design, thermal design, magnetic shielding, and design of the anticoincidence detector. This is described in detail in [Jackson et al. 2016], and referenced within.

An FPA using microwave SQUID resonators will be similar to that of the X-IFU in many ways, but parts of the design are different and need to be proven. For example, the LXM has higher estimated heat loads at 50 mK. This difference has allowed us to consider mechanical support of the 50-mK stage that uses fiberglass thrust tubes to support the 50-mK stage from the 0.6-K stage, and the 0.6-K stage from the 4.5-K stage, instead of the more traditional approach of using low-thermal-conductivity Kevlar strings.

2.4.3 Interconnects

From the HEMTs at 4.5 K to the detectors at 50 mK, the options for the cabling are small-diameter superconducting coaxial cables that are in widespread use and microstrip on Kapton microwave flex, as has been demonstrated in a few laboratories (e.g., [Harris et al. 2012]). Superconducting versions of such microwave flex should be feasible. The requirements can be met using coax, but if the flex is developed, it will increase the margin relative to the thermal requirements. Standard semi-rigid coaxial cables will be used between the HEMTs and room temperature.

Another critical issue is how to make connections between the TES sensor wires on the detector chip, and the microwave SQUID readout chips. This requires routing the signals around a corner to keep the FPA mass low and magnetic shielding less complex. These signals are only in the tens of kHz range and therefore do not require GHz flex; however, they do require something like a flex with microstrip geometry to maintain sufficient immunity to electromagnetic induction pick-up and to maintain a small footprint. Several groups have developed such microstrip flex for the readout of TESs.

2.4.4 Bump Bonding

To make contact at each end of the flex (see §2.4.3), bump bonding is the most reliable and well-established technology (TRL 5) for large arrays. Indium bonding for cryogenic instruments for spaceflight and airborne astronomy has been implemented in FPAs and is a high-yield process [Li et. al. 2007; Jhabvala et. al. 2016]. High critical-current indium superconducting interconnects needed for full characterization of TES focal planes are in development for *Athena*'s X-IFU [DeNigris et al. 2018] and are currently TRL 4, with a full-scale demonstration planned in the coming year. The *Lynx* focal plane will leverage this development effort which is on pace to mature the technology in time for the first full-scale *Lynx* FPA prototypes.

2.4.5 Infrared/Optical Blocking Filters

The blocking filters, typically built using aluminized polyimide films that are either freestanding or supported by a mesh, need to have thin films to enable soft X-ray transmission. Most microcalorimeter instrument designs require between 4 and 7 filters mounted at various temperatures within the cryostat. The filters are mounted in a carefully designed aperture assembly. This filter technology is well proven through the development of filters for laboratory systems, sounding rocket experiments, and for *Astro-H*. For the LXM, these filters will need to be larger; however, the LXM filters are comparable in size to those needed for *Athena*'s X-IFU, and the design will benefit greatly from the X-IFU development efforts.

The LXM filters will provide greater transmission at low X-ray energy compared to the X-IFU, since some of the most important *Lynx* science comes in the region below 1 keV. Research groups are actively pursuing both incremental and potentially groundbreaking technology developments to increase the throughput at low energies while baselining traditional components at TRL 5 [Eckart et al. 2019].

2.5 Element 4 – Cryogenics

2.5.1 Cryostat Design

State of the Art—At this time, there is no need for the development of prototype LXM cryostats. It will be sufficient to carry out paper studies based upon various cryostat design options. Many cryostats have already been developed for space-based applications, and many cryocoolers that integrate into them are under development. As the *Lynx* FPA develops, the cryocooler definition improves, the vibration requirements are refined, and designs that are more detailed will be needed. One concern is how close other instruments such as the gratings readout needs to be to the axis of the FPA. Optimization of the cryostat design in terms of the thermal design, vibrational isolation, and desired physical geometry will evolve as the LXM design is refined.

The non-TRL-related activities that will occur in Phase A include working with space cryogenics experts in industry and at NASA Centers to refine the LXM design and developing a mechanical model of cryostat to determine the FPA vibrations level through simulation.

Toward the end of Phase A, the building of a structural thermo-model of the cryostat (to be confirmed) will start. After completion in Phase B, it will be integrated with the TRL 6 ADR and FPA to investigate interferences between these subsystems.

2.5.2 Cryocoolers

A wide variety of cryocoolers exist that, in principle, can meet the LXM cooling requirements to 4.5 K. The most desirable cryocoolers are the simplest, dissipate the least power, generate the lowest vibration levels, are the most reliable, and are already at the highest TRL levels. The current 4.5-K cryocooler technology ranges between TRL 3 and TRL 7, depending on the vendor and technology.

We have chosen to focus on two of these possible cryocoolers: the Lockheed Martin multistage pulse tube cryocooler and the Creare miniature Reverse-Brayton-cycle cryocooler. Note that this development is synergistic with similar requirements for 4.5-K cryocoolers for far-IR missions. 4.5 K is also required as a precooler for many other types of detectors cooled to sub-Kelvin temperatures.

Lockheed Martin Pulse Tube — The Lockheed Martin cryocooler is a 4-stage pulse tube cryocooler based on the design built and tested as part of the ACTDP 10. The cryocooler will use the same Lockheed Martin "Mega" compressor used on ACTDP, with a compressor mass of 18 kg and a 4-stage cold head (similar to the ACTDP cold head), but with dimensions modified in order to optimize performance at the required *Lynx* cooling temperatures and loads. The compressor is a long-life "Oxford-style" compressor utilizing flexure bearings and clearance seals, with a simple moving magnet motor configuration that allows the motor coils to be external to the pressure vessel, a configuration that minimizes organics within the working fluid and eliminates electrical penetrations through the pressure vessel. The cold head has no moving parts, and has all metal sealing for long life gas retention.

The Lockheed ACTDP cryocooler was designed to provide 20 mW cooling at 6 K and 150 mW at 18 K, which required 208 W of AC compressor electrical power during testing. The LXM temperatures are colder and the heat loads higher than ACTDP, so the required input power is higher, currently estimated to be 555 W plus an estimated 98 W dissipated in the electronics for a total power of 653 W to be supplied by the spacecraft bus. A future higher efficiency compressor that is not yet available could lower the power needed to 453 W, or 533 W bus power, but for now, the higher power number for the LXM is conservatively assumed. The LXM cryocooler mass is estimated to be 25 kg, with an additional 10 kg for the control electronics.

To meet the demands of the full preliminary cryostat design, this cooler will provide 3.6 W of cooling at 80 K, 180 mW of cooling at 40 K, 65 mW of cooling at 15 K, as well as the 50 mW of cooling at 4.5 K. The use of commercially available flight electronics has been used for our cost and mass of estimate, such as the type developed by IRIS, which are at TRL 5; some new parts selections may be needed to accommodate the L2 environment. The same Mega compressor was used for a different program and was tested with as much as 800 W of AC electrical input power, and therefore is sufficiently powerful to provide the cooling for LXM. The cryocooler cold head will use the same staging configuration as the ACTDP 4-stage cooler. This configuration is robust and straightforward to design, assemble, and test. The LXM cold head may be required to support significant masses during launch vibration, so design iterations are expected in order to meet minimum resonant frequency requirements. Lockheed Martin has performed similar design iterations on other multiple-stage coolers.

2.5.3 Adiabatic Demagnetization Refrigerators

State of the Art — 50-mK cooling has been demonstrated on *Hitomi* by an ADR lifting 0.4 μW from the detector array. This could be considered TRL 7. To achieve 6 μW of cooling, as is currently

baselined for the LXM, a Continuous ADR (CADR) will be needed. This refrigerator has been demonstrated at TRL 4. There is a current technology development effort to raise the TRL of this CADR to TRL 6 that is funded by a SAT grant though 2019. For LXM, with a separate continuous stage operating at 0.6 K, this CADR has four stages operating between 4.5 K and 50 mK. For LXM, a fifth stage operating continuously at 0.6 K must be demonstrated.

2.6 Key Milestones

The Advancement Degree of Difficulty (AD^2) to reach the next TRL level is identified in Table 7. See §4.2 for more information on AD^2.

Table 7—LXM TRL 4–6 Milestones.

TRL3=>4 Advancement Degree of Difficulty: The two key technologies requiring development to reach TRL 4 are the detectors and readout. We expect this development will be completed within the next several months under existing programs. For the TES detectors, the degree of difficulty is AD2= 2/3 because there already exist arrays with properties that are well understood and meet the TRL 4 criteria. The remaining TRL milestones involve measuring these arrays in standard testing configurations (e.g., with appropriate Nyquist inductors) similar to demonstrations that have been successfully completed for Athena. The parallel MMC detector technology is desirable for eventually achieving even better (goal) performance, with the potential for easier calibration. For MMCs, the AD2= 3/4 as MMCs have further to go to demonstrate Ultra-Hi-Res Array pixel performance, and require additional readout development optimization. For umux readout, the AD2= 3 as design optimization is needed to match the bandwidth requirements of the LXM detectors; however, existing experimental demonstrations have provided proof of concept for all aspects of the expected design. The CDM readout technology development is a parallel option again more important for optimization potential at system level (higher TRL level). For TRL 4, adapting the current CDM designs for the properties of the LXM detectors is relatively straightforward (AD2= 2). Existing FPA, filters, and cryogenic technologies meet TRL 4 criteria. One cryocooler option currently has a component at TRL 3; this back-up option is being pursued as it could be useful later for system-level demonstrations, reducing vibrations.
Anticipated date to achieve TRL 4: 6/30/21 (with most development completed in 2020 or before)

NASA TRL 4	**A low-fidelity system/component breadboard is built and operated to demonstrate basic functionality and critical test environments, and associated performance predictions are defined relative to the final operating environment.** **Breadboard: A low-fidelity unit that demonstrates function only, without respect to form or fit in the case of hardware, or platform in the case of software. It often uses commercial and/or ad hoc components and is not intended to provide definitive information regarding operational performance.**

LXM TRL 4 Exit Criteria	**LXM Development/Maturation Milestones**		
	#	**Milestone Description**	**Date**
A low fidelity breadboard system/component must demonstrate a credible technology development path to the required on-orbit performance of the LXM. Demonstrations must be traceable to the on-orbit performance requirement in the operational environment. System/component performance is consistent with the expected flight performance, given no worse than a 50% uncertainty in lab demonstrations and models, unless otherwise noted, consistent with the low-fidelity system required for TRL 4.	1	Microcalorimeter Pixel Arrays	
	1.1	Demonstrate 25-absorber hydras on 50-μm pitch with suitable signal time constants with appropriate Nyquist inductances. Performance shall demonstrate ΔE_{FWHM} <4 eV at 6 keV, and position discrimination down to 1.5 keV.	12/1/2019
A credible demonstration must include the following: **A credible sensor performance budget**	1.2	Demonstrate 25-absorber hydras on 25-μm pitch with suitable signal time constants with appropriate Nyquist inductances. Performance shall demonstrate ΔE_{FWHM} <3 eV at 6 keV, and position discrimination at 1.5 keV.	12/1/2019

Laboratory demonstrations: For the detector, the operation of each of the three detector subarray pixel types should be demonstrated with form-factors (pixel size, pitch, and quantum efficiency) and performance (pitch, energy resolution, energy range). Specifically, they should meet the following characteristics and performance:	1.3	Demonstrate single-pixel detector array with pixels of 50 μm pitch ΔE_{FWHM} <0.5 eV (Ultra-Hi-Res Array) at photon energies below 1 keV, with suitable signal time constants with appropriate Nyquist inductances.	12/1/2019
	2	Microcalorimeter Readout	
• Multi-pixel detectors (hydras) demonstrated with absorber pitches 50 and 25 μm, with 25 absorbers attached to each sensor, demonstrating <4 eV and <3 eV energy resolution [FWHM] up to 6 keV (Main Array and Enhanced Main Array, respectively).	2.1	Design and fabricate microwave SQUID circuitry with the appropriate noise level and resonator bandwidths and resonance frequency spacing for the LXM microcalorimeters.	10/1/2019
• Single-pixel detector array with pixels of 50-μm pitch demonstrating an energy resolution of <0.5 eV (FWHM) (Ultra-Hi-Res Array).	2.2	Demonstrate readout of the relevant pixel types at reduced multiplexing factors with energy resolution degradation from the readout of less than 30% of single pixel readout.	10/1/2020
• Demonstrate the required performance with appropriate wiring density for all pixel types.	2.3	Demonstrate readout of relevant pixel types with energy resolution degradation from the readout of less than 30% of single pixel readout at relevant multiplexing factors.	12/31/2020
For the readout, the microwave SQUID prototypes need to demonstrate that they are capable of reading out the three different pixel types. Specifically, a demonstration of the readout should meet the following characteristics and performance:	2.4	Demonstrate CDM circuitry that provides appropriate noise, switching speeds, input channel count, and circuit yield.	3/1/2020
• Representative readout architecture.	2.5	Demonstrate the relevant pixel types using CDM integrated with an error correction capability.	10/1/2020
• Demonstrate required microwave SQUID circuitry with appropriate noise and resonator widths and spacings. • Degradation on intrinsic energy resolution of microcalorimeters (any type) less than 30% of what can be achieved with single-pixel readout. • Demonstrate basic functionality of the assumed LXM HEMT amplifier architecture. • At realistic operating temperature and using laboratory electronics.	2.6	Demonstrate readout of relevant pixel types at relevant multiplexing factors using CDM.	12/2/2021
As a system-level bread-board demonstration: • Using arrays to meet detector and readout sub-system level requirements, demonstrate the readout of at least 100 sensors (Main Array hydras in one demonstration, Ultra-Hi-Res Array single pixels in a second) read out simultaneously on a single readout channel, with representative energy resolution.	2.7	Analyze HEMT architecture and identify the production path and a path to produce flight qualified HEMTs.	7/1/2020
• At realistic operating temperature and using laboratory electronics.	2.8	Demonstration of HEMT architecture (a single HEMT amplifier).	12/31/2020
Model predictions: • Refined models of each of the three pixel types, based upon measured pixel parameters in the three subarrays, must meet LXM performance requirements.	2.9	Assemble appropriate room temperature readout electronics using commercial parts as a breadboard model spanning a bandwidth of 1–2 GHz (these electronics do not need to be coupled to low-temperature readout components).	10/1/2020

• The electronics will be able to readout the pixel types with properties given by detector modelling of each of the three subarrays needed by the LXM, assuming a number of readout channels that are feasible within the cooling system and preliminary FPA designs. • Radiation effects on flight arrays and readout are demonstrated to not degrade performance beyond requirements for dosage expected at L2 with 5 years of operation.	2.10	With the COTS room temperature electronics (described in TRL 4-2.3.1), demonstrate readout of relevant pixel types at relevant multiplexing factors over a 1–2 GHz bandwidth using microwave SQUID multiplexer components.	12/31/2020
	2.11	For MMC readout, demonstrate sufficiently low coupled energy sensitivity, high enough input inductance, and reduced lithographic area per SQUID, to enable the readout of MMCs with <30% degradation of energy resolution compared with single-pixel readout.	10/1/21
	4	Cryogenics	
	4.1	Demonstrate 4.5 K Reverse-Brayton cryocooler system-level performance in a laboratory environment. (SBIR Phase II ongoing)	6/30/21
TRL 4=>5 Advancement Degree of Difficulty: For the detectors AD^2= 2/3. The only technical advancement is the need to heatsink, and approaches will be followed similar to designs that have previously demonstrated the necessary level of heatsinking. Scale-up is no issue due to the already included buried wiring technology. For the readout, AD^2= 4 as there is some new development needed. However, this development is identical to that need by a wide variety of detectors for terrestrial applications, and so there is a whole community supporting this effort that provides a high degree of confidence of success. For the FPA and filters, the AD^2= 2 because very little new technology is necessary beyond what has been demonstrated for the *Athena* X-IFU. The only new innovation involves the use of an FPA support structure that is mechanically straightforward, an approach made possible by the CADR and the relatively high cooling power it offers. The filters are already sufficient, and will simply be further optimized for higher throughput in pre-Phase A. For the cryocooler, AD^2= 4 for each of the cryocooler options because the new versions proposed require some development on a short timescale since the requisite funding level is not expected until pre-Phase A. Based upon the existing development, each has a high degree of confidence of success, but this step is key to the success of either cryocooler option.			
Anticipated date to achieve TRL 5: 12/31/23			

NASA TRL 5	**A medium fidelity system/component brassboard is built and operated to demonstrate overall performance in a simulated operational environment with realistic support elements that demonstrate overall performance in critical areas. Performance predictions are made for subsequent development phases.** **Brassboard: A medium fidelity functional unit that typically tries to make use of as much operational hardware/ software as possible and begins to address scaling issues associated with the operational system. It does not have the engineering pedigree in all aspects, but is structured to operate in simulated operational environments in order to assess performance of critical functions.**		
LXM TRL 5 Exit Criteria	**LXM Development/Maturation Milestones**		
	#	**Milestone Description**	**Date**
Must demonstrate a credible technology development path to the required on-orbit performance of the LXM array. Demonstrations must be traceable to the on-orbit performance requirement in the operational environment. Performance is consistent with the expected flight performance, given no worse than a 30% uncertainty in lab demonstrations and/or models, consistent with the medium-fidelity system required for TRL 5.	1	Microcalorimeter Pixel Arrays	
	1.1	Demonstrate full-scale hybrid array of the appropriate format, area, and wiring all pixels of a full-scale array including all three pixel array types.	12/31/2023
A credible demonstration must include the following:	1.2	Demonstrate that detector performance is not degraded beyond the energy resolution budget after a radiation dose equivalent to 5 years at L2	12/31/2023
For the detector subsystem, operation of each of the three detector subarray pixel types should be demonstrated with form-factors (pixel size, pitch, and quantum efficiency) and performance (pitch, energy resolution, energy range) that meets the energy resolution budget requirements for the detector subarrays of the LXM.	1.3	Demonstrate process for detector embedded heatsink layer.	12/31/2023

• Format, area, and wiring all pixels of a full-scale array is needed. • Pixel yield meeting requirements needs to be >85%.	2	Microcalorimeter Readout	
	2.1	Demonstrate readout of all relevant pixel types at required multiplexing factors across the full bandwidth with energy resolution within the error budget allocation.	12/31/2023
• Prototype detector will demonstrate that performance is not degraded beyond the energy resolution budget after a radiation dose equivalent to 5 years at L2.	2.2	Demonstrate microwave SQUID multiplexer circuit performance is not degraded by more than allocated by the resolution budget for dose equivalent to 5 years at L2.	10/1/2023
For the readout, the microwave SQUID readout needs to demonstrate that it is capable of reading out the three different pixel types and agree with expected performance within the energy resolution budget. Specifically, a demonstration of the readout should meet the following characteristics and performance:	2.3	Demonstrate code-division multiplexer circuit performance is not degraded by more than allocated by the resolution budget for radiation dose equivalent to 5 years at L2.	10/1/2023
• Representative readout architecture.	2.4	Demonstrate CDM readout of required pixel types at a representative number of columns with energy resolution degradation within error budget allocation.	6/1/2023
• Demonstrate required microwave SQUID circuitry with appropriate noise and resonator widths and spacings.	2.5	Demonstrate HEMT architecture and appropriate cabling (three or more HEMTs in a flight-like configuration, each connected to appropriate cabling).	10/1/2023
• The yield of functioning readout of all pixels meeting all noise and input slew rate requirements is >85% • Demonstrate exact functionality of the assumed LXM HEMT amplifier architecture. • Prototype readout chips will demonstrate that performance is not degraded beyond the energy resolution budget after a radiation dose equivalent to 5 years at L2.	2.6	Assemble room temperature readout electronics as a brass-board model using flight-qualified parts or non-flight parts when a flight-qualified version of the parts exists or are undergoing the NASA space qualification process.	10/1/2022
• At realistic operating temperature and using laboratory electronics. • Functional prototype electronics exist that uses flight-compatible components (or commercial components where flight-compatible versions exist), meeting the functional and expected power/mass envelopes for the LXM.	2.7	Demonstrate isolated readout of relevant pixel types at relevant multiplexing factors at frequencies ranging over the full range of bandwidth of the HEMT (typically 4 GHz) using a room temperature readout electronics system built with flight-qualified parts or non-flight parts when a flight-qualified version of the parts exists or are undergoing the NASA space qualification process.	6/30/23
A representative FPA needs to be demonstrated that allows the mounting of a full-scale detector and anti-coincidence detector, and is sufficiently large to accommodate readout of required number of readout channels.	2.8	Demonstrate simultaneous readouts of relevant pixel types at relevant multiplexing factors over a full range of bandwidth of more than two HEMT channels (typically 4 GHz per HEMT) using a room temperature readout electronics system built with flight-qualified parts or non-flight parts when a flight-qualified version of the parts exists or are undergoing the NASA space qualification process.	9/31/23
Specifically, it must: • Demonstrate that it can withstand the vibrations expected from the *Lynx* launch.	2.9	Demonstrate that the heatsinking between the PCB and chassis is adequate to dissipate the heat generated from the high-power components (FPGA, ADC, and DAC).	12/31/23
• Demonstrate wiring/cabling at the density needed for wiring out the entire array.	2.10	Develop board support equipment (BSE) / ground support equipment (GSE) for a signal emulator for the cold electronics and test the developed system to ensure it meets the full requirements.	12/31/23
• Demonstrate sufficient heatsinking of the detector and readout.	3	Focal Plane Assembly	

A cooling system needs to be demonstrated that meets typical TRL 5 level cooling requirements. Specifically: • A 4.5 Kelvin cooler (TRL 5) needs to be demonstrated meeting its cooling requirements. • A TRL 5 multi-stage adiabatic demagnetization cooler needs to be demonstrated meeting the cooling requirements at 50 mK and 1.0 K, generating less than 5 mW at 4.5 Kelvin.	3.1	Determine kinematic mounting approaches for the Main Array and anti-coincidence detector, and the microwave SQUID resonator chips together with Nyquist inductors and bias resistors.	12/31/23
	3.2	Perform simulations and experiments to determine whether there will be issues related to RF signals interfering with each other among the different microwave SQUID resonator chips. Demonstrate readout of all relevant pixel types at required multiplexing factors with energy resolution within the error budget allocation.	10/1/22
Laboratory demonstration of a brassboard sensor array with the following characteristics and performance:	3.3	Verify the thermal and mechanical properties of the T-300 cone-shaped thrust tubes used for mechanical support of the FPA between different temperature stages, and verify the mechanical properties and the DC- and AC-shielding performance of the magnetic shields.	10/1/23
• Arrays meeting detector requirements and readout sub-systems meeting all TRL 5 requirements; demonstrate the readout of required numbers of sensors (Main Array hydras in one channel, Enhanced Main Array hydras in a second, and Ultra-Hi-Res Array single pixels in a third) read out simultaneously on three readout channels, with energy resolution meeting the required performance of all the detectors.	3.4	Calculate appropriate coaxial cable design (lengths) needed for the stages at 4.5 K and below, given known thermal conductance and mechanical properties, and the relevant LXM requirements. Design superconducting flex for the around-the-corner wiring between the sensor arrays and the microwave SQUID multiplexer (with number of traces appropriate for LXM). Build appropriate cables and measure thermal, mechanical, and electrical properties.	10/1/23
• A representative (TRL 5) FPA.	4	Cryogenics	
• Assembly that includes a cryogenic system and realistic support structure.	4.1	Design, fabricate, and demonstrate a pulse tube cryocooler system with breadboard electronics using flight-compatible electronics components and verify that the system meets performance requirements and is compatible with expected launch loads.	9/1/23
• X-ray test demonstrating feasibility of achieving *Lynx* performance requirements in simulated operational environment.	4.2	Design system with appropriate support structure and perform vibration testing and post vibration performance testing to demonstrate survival of launch loads for the 4.5K Reverse-Brayton cryocooler system.	9/1/23
• Realistic operating temperature using laboratory electronics.	4.3	Demonstrate performance and meeting of launch load vibrational requirements. Verify sufficient reliability of all ADR heat switches, and salt pill suspensions within the CADR. Verify low external magnetic field (<30 μT).	4/31/23
Model Predictions: • Models/predictions verify the full-scale LXM meets the required mass, volume, and power envelopes			
TRL 5=>6 Advancement Degree of Difficulty: For the detectors, AD^2= 2, as once again the development needed is only minor due to the already advanced, large-scale demonstration of fabricating the detectors successfully. Once TRL 5 is established, the detector essentially already exists, and yield and sensitivities to the environment need to be verified, which aren't expected to be problematic. The readout scale-up at low temperatures will require new development to integrate into the new FPA geometry and is given an AD^2= 4. The room temperature electronics have a clear and feasible plan of development, but require a significant amount of engineering support at this stage. This scale-up is not risky, but requires a large effort over a relatively short period of time. The FPA development is key at this stage and also represents a large engineering effort. Without *Athena*, this would be a very large effort, but since we plan to leverage much of the similar *Athena* FPA design, we expect this will be straightforward AD^2= 3. The cryocooler advancement from TRL 5 to TRL 6 is expected to be straightforward, with mostly testing needed on the demo cryocooler developed for TRL 5.			
Anticipated date to achieve TRL 6: 2/28/26 for detectors and readout, 6/1/27 for the rest of the instrument.			

NASA TRL 6	**A high-fidelity system/component prototype that adequately addresses all critical scaling issues is built and operated in a relevant environment to demonstrate operations under critical environmental conditions.** **Prototype: The prototype unit demonstrates form, fit, and function at a scale deemed representative of the final product in its operational environment. A subscale test article provides fidelity sufficient to permit validation of analytical models capable of predicting the behavior of full-scale systems in an operational environment.**

LXM TRL 6 Exit Criteria

Must demonstrate using a high-fidelity, scalable, flight-like prototype, which adequately addresses all critical scaling issues and that meets all *Lynx* performance requirements in critical environments.
A TRL 6 prototype system will be demonstrated for the LXM:

Prototype Characteristics:

- A full-size flight-like array; pixel yield requirements needs to be > 95%
- A full set of cold, flight-like readout electronics for all channels including a full set of HEMTs at 4.5 Kelvin. The yield of functioning readout of pixels meeting all noise and input slew rate requirements is >95%.
- A full-size, fully populated mechanical prototype FPA.
- Meeting all detector/readout error budget requirements
- A TRL-cooling system including a TRL 6 cryocooler and multi-stage ADR.
- At realistic operating temperature.
- Use of flight-compatible electronics that uses flight-compatible components (or commercial components where flight-compatible versions exist), meeting the functional and expected power/mass envelopes for the LXM with sufficient boards to read out a half of the array.
- A representative event processor operating at required rates.

Environmental testing:

- Acoustic (blocking filter only), thermal vacuum, vibration, radiation, and X-ray testing, as appropriate, in operational environments.

LXM Development/Maturation Milestones

#	Milestone Description	Date
1	Microcalorimeter Pixel Arrays	
1.1	Demonstrate that a full-size, flight-like array has a pixel yield meeting requirement of >95%.	2/28/26
1.2	Demonstrate all detector/readout error budget requirements are met.	6/1/27
1.3	Demonstrate that cosmic-ray background events will not cause degradation of performance.	2/28/26
2	Microcalorimeter Readout	
2.1	Demonstrate a quarter set of cold, flight-like readout electronics for all channels including a full set of HEMTs at 4.5 K. The yield of functioning readout of pixels meeting all noise and input slew rate requirements is >95%.	2/28/26
2.2	A full-scale readout system needs to be designed, constructed, and tested using flight-qualified parts or non-flight parts when a flight-qualified version of the parts exists. This system should be assembled in a realistic form factor.	6/1/27
3	Focal Plane Assembly	
3.1	Design, build, and test a full-scale FPA attached to a continuous ADR to provide representative temperatures/conditions for FPA operation. This will include appropriate interconnects (Element 3.2) and bump bonding (Element 3.3).	2/28/26
3.2	Build a set of blocking filters compatible with the FPA and cryostat design, including with appropriate kinematic mounts. Demonstrate in the relevant environments using a vibration table for mechanical verification and deployment in a cryostat to demonstrate thermal and magnetic shielding requirements.	6/1/27
4	Cryogenics	
4.1	Design a cryostat that meets the thermal and structural requirements of LXM. Perform structural and/or thermal sample tests where suitable data for specific materials used in the design does not currently exist. (Note, that right now LXM anticipates using materials with known properties.)	6/1/27
4.2 and 4.3	(Cryocooler) Demonstrate full system and perform environmental testing, including tests of the electronics. The design must be compatible with LXM mechanical requirements (for example, fit within the cryostat housing).	6/1/27
4.4	Verify complete 5 stage design including 0.6 K continuous stage, and demonstrate full system performance (including flight-like electronics) meets LXM requirements.	10/1/24
4.5	Demonstrate 6 mW cooling at 50 mK. Increase size of components of the CADR and increase suspension strength and stiffness. Perform launch loads testing and verify performance.	10/1/24

2.7 Milestone Details

Milestone details are laid out for each of the four major elements for the LXM. Element 1 lays out each of the TRL milestones, their significance, and verification of the subelements for the pixel arrays. Element 2 provides the TRL milestones for the microcalorimeter readout, Element 3 the FPA and filters, and Element 4 the cryogenics.

2.7.1 Element 1—Large Format, High Spectral Resolution Microcalorimeter Pixel Arrays

2.7.1.1 TRL 4 Element 1.1—Microcalorimeter Arrays

Milestone TRL 4-1.1 — Demonstrate that 25-absorber hydras with 50 μm pitches can achieve <4 eV energy resolution with required signal time constants and Nyquist inductances at 6 keV, and position discrimination will be demonstrated down to 1.5 keV.

Significance—Needed for the LXM Main Array. The hydra resolution performance to date has been evaluated on designs with 20% fewer pixels than the design goal. These original designs have been modified to accommodate an additional five absorbers and performance tests have begun. In order to achieve TRL 4, it is important to show the required performance can be achieved in a design that is compatible with the proposed readout scheme. TESs are typically operated in or close to critical damping whereby a large inductance is placed in series with the detector. This is used to reduce the speed of the pixels, which in turn reduces the bandwidth and dynamic range requirements of the readout. This is usually parameterized by the maximum current slew rate, dI/dt, which occurs at the maximum photon energy of interest. In the hydra design, it is the pixel thermally coupled directly to the TES that has the fastest rise-time and therefore the largest slew rate. Although some inductance can be used to reduce the slew rate, it is undesirable to critically damp the hydra since this would suppress the high-frequency signal-to-noise ratio required for position discrimination. In these initial hydra designs for LXM, the first pixel is coupled directly to the TES, making the resulting slew rates fast. These initial designs are being used to verify the yield and characterize the performance properties of the basic hydra design (verify conductance of thermal links, device heat capacity, TES transition temperature, etc.) and they are not anticipated to be suitable for readout demonstrations.

For the next LXM design iteration, the optimal slew rate to match the bandwidth of the readout will be achieved by thermally decoupling the TES from all pixels. In order to achieve the desired time constant and slew rate, the heat capacity of the TES will be increased by an order of magnitude by incorporating a high specific heat Pd layer (×20 higher C compare to Au) connected to the TES and by introducing a thermal link to thermally decouple the first pixel. This comes with only a modest decrease in resolution performance. These designs are currently being drawn, and devices will be fabricated and tested through the end of FY19. After initial performance tests of the resolution and slew rate, another design iteration is anticipated for later in 2019 to further tune internal thermal design.

Verification—The hydra energy resolution, position resolution, and slew rate will be experimentally evaluated over a range of energies and compared against numerical simulation. Measurements will be carried out using a range of different Nyquist inductors to evaluate the optimum choice of inductance for readout demonstrations.

Milestone TRL 4-1.2 — Demonstrate that 25-absorber hydras with 25 μm pitches can achieve <3 eV energy resolution with required signal time constants and Nyquist inductances at 6 keV; position discrimination will be demonstrated down to 1.5 keV.

Significance—Needed for the LXM Enhanced Main Array. Milestone significance is essentially the same as the Main Array hydras described previously, and the pixel design optimization approach is the same. Since the pixels are smaller (lower heat capacity), the predicted energy resolution is better than the Main Array, but the slew rates are faster, thus the pixels are being designed to match the higher bandwidth (8 GHz) μMUX chips.

Verification—The hydra energy resolution, position resolution and slew rate will be experimentally evaluated over a range of energies and compared against numerical simulation. Measurements will be carried out using a range of different Nyquist inductors to evaluate the optimum choice of inductance for readout demonstrations.

Milestone TRL 4-1.3 — Demonstrate that single pixels on a pitch of 50 μm have an energy resolution <0.4 eV at energies <1.0 keV with suitable signal time constants with appropriate Nyquist inductances.

Significance—Needed for the LXM Ultra-Hi-Res Array. Initial performance testing has been carried out on prototype Ultra-Hi-Res Array pixels. Tests using a fluorescence X-ray target source at 1.5 keV demonstrated a highly nonlinear response and an energy resolution of ~2.2 eV. Since this is significantly higher than the top end of the required resolution performance (0.8 keV) follow-up tests focused on the low-energy response. The energy resolution demonstrated 0.26 eV for optical fiber coupled UV photons at an energy of 3 eV. This is comparable to resolution requirements. The heat capacity of these pixels was ~2× larger than the original design goal. Thus, devices with the original heat capacity target may have sqrt(2) better resolution at low energies but may become more nonlinear at higher energies. In these initial measurements, the photon energy range was limited to 3 eV only, but future optimization of the experimental setup should allow calibration up to hundreds of eV. Follow-up tests on these devices are now planned to verify the linearity of the resolution response up to a photon energy of 1 keV, with further tests to be carried out on devices that will be fabricated with ~2× lower heat capacity. These tests will be carried out at a University of Wisconsin –Madison test facility where they have a more optimized test setup for UV diode calibration testing. Initial testing in the UW-Madison facility is planned for mid-2019 and will continue through mid-2020. At the same time, the GSFC test facility will be upgraded to enable similar tests over the longer term.

Verification—The energy resolution and slew rate will be experimentally evaluated for photon energies up to 1 keV and results compared against numerical simulation. Measurements will be carried out using a range of different Nyquist inductors on devices with different heat capacities to evaluate the optimum design choice for subsequent readout demonstrations.

2.7.1.2 TRL 5 Element 1.1—Microcalorimeter Arrays

Milestone TRL 5-1.1 — Fabricate hybrid arrays consisting of all required pixel types.

Significance—Over the past few years, various techniques have been developed that prove the feasibility of using a hybrid TES array consisting of different pixel types on a single substrate [Wassell et al. 2017]. A demonstration hybrid array was fabricated that consisted of 50-μm single pixels in the central region,; 50-μm-pitch, 9-absorber hydras in the next region around it; and 100-μm-pitch, 9-absorber hydras in a third outer region. We have already shown that pixels requiring different

compositions of absorbers (with coupling to the heatsink) can be fabricated in the same array. These techniques are being used to fabricate arrays that incorporate the three different proposed array types (Main Array, Enhanced Main Array, Ultra-High-Res array) on a single fabricated die. Prototype arrays, including all three pixel types in a single detector chip have already been yielded. These arrays include around half the number of pixels of the proposed full-scale array. In these first wafers, the absorber composition was uniform for all pixel types. The original design goal was for 4-μm-thick Au in the Main Array and Enhanced Main Array, with only 1 μm in the Ultra-Hi-Res Array, thus process development is underway in order to incorporate different absorber composition in these different arrays. The fill factor for each pixel will depend upon the gaps between absorbers. How narrow this gap can be depends upon the thickness of absorber. In first prototype arrays, the gaps between absorbers were 4 μm, which we can achieve for a 4-μm-thick Au. Optimization of the ion-milling process should allow the absorber gaps to be reduced below 2 μm.

Verification—In order to verify this milestone, a full-scale array must be produced with appropriate form, quantum efficiency, and pixel uniformity properties for all three subarrays in a single chip.

Milestone TRL 5-1.2 — A prototype detector will demonstrate that performance is not degraded beyond the energy resolution budget after a radiation dose equivalent to 5 years at L2.

Significance—An important TRL 5 component is to validate the relevant space radiation environment. For radiation testing, there are two effects to consider: physical damage and driving a superconducting element locally normal.

Verification—We propose to irradiate previously characterized arrays at a proton facility such as University of California–Davis to see if there is any measurable evidence of damage. Separate X-ray tests will be carried out to examine the impact of local heating in the buried bias leads.

2.7.1.3 TRL 6 Element 1.1—Microcalorimeter Arrays

Milestone TRL 6-1.1 — Demonstrate that a full-size, flight-like array has a pixel yield meeting the requirement of >95%.

Significance—For the LXM array, the pixels need sufficient yield and performance uniformity that the effective area of the measurements are not unacceptably degraded due to insufficient pixels functioning and meeting requirements.

Verification—Pixels in a demonstration array will be scanned at various stages of the fabrication process to verify that the yield due to fabrication defects meets requirements. With the operation of a quarter of the LXM array (including a quarter of each subarray), verify that a sufficiently large fraction of the pixels meets all the pixel requirements, and that the overall yield of the array is >95%.

Milestone TRL 6-1.2 — Demonstrate all detector/readout error budget requirements are met.

Significance—It is important to verify that all error budget terms are met by the detector and readout to know that the performance of the instrument on-orbit will meet requirements. This includes verifying that the performance under assumed environmental conditions and stability of conditions (e.g., temperature magnetic field, Electromagnetic Interference (EMI) susceptibility, micro-vibrations, etc.) will meet the individual performance error budget terms.

Verification—Verify that the performance of the detector and readout remains within the thresholds established for the error budget terms for the size and variation of each relevant external environmental condition.

Milestone TRL 6-1.3 — Demonstrate that cosmic-ray background events will not cause degradation of performance.

Significance—The detector wafer will absorb energy depositions in orbit due to cosmic rays (and secondaries) passing through the detector substrate. The heatsinking design needs to be sufficiently strong that the cosmic ray events do not cause energy resolution degradation.

Verification—The cosmic ray energy flux and spectrum and the variation in time can be estimated through modeling. The effects on the detector can also be modeled through an end-to-end simulation, as has produce for the *Athena* X-IFU. The effects of representative energy depositions on the performance of detectors (such as from alpha particles) will be verified to smaller than the error budget term associated with this effect, when results from monoenergetic depositions are scaled to represent the effect of the entire cosmic ray spectrum.

2.7.1.4 TRL 5 Element 1.2—Buried Superconducting Wiring

Milestone TRL 5-1.3 — Demonstrate heat inking of arrays with buried wiring.

Significance—One unknown in designing large arrays with buried multilayer wiring is how the wiring stack will behave thermally and mechanically. Even though wires will not be routed directly under the TES, it will sit on the stack of separate insulating layers put down to isolate the various metal layers. In order to minimize thermal gradients and crosstalk, each TES needs to be coupled to a backside heatsinking layer. In general, a heat bath consisting of a continuous highly conductive metal film directly below the wiring and pixels is ideal. The benefits of buried metal heatsink layers has been show before [Finkbeiner et al. 2011], and the feasibility of incorporating in hybrid arrays of differing pixel types has already been demonstrated [Wassell at el. 2017]. A process is now being developed to incorporate SiN membranes into the multilayer LL stack. The Si directly under each TES can then be removed and a metal heatsink layer deposited directly against the SiN insulator. The incorporation of a SiN layer into the LL multilayer stack is planned for FY19. The back etching and backside metal layer deposition and first performance verification will be carried out at GSFC in late FY19/FY20.

Verification—The internal heatsinking will be verified in full-scale arrays by biasing a substantial fraction of pixels within the array and comparing performance to tests with very few biased pixels. The analysis will be compared to COSMOL simulation of the anticipated internal temperature gradients within the array.

The thermal crosstalk will be evaluated through X-ray crosstalk and energy resolution measurements at count rates and energies consistent with *Lynx* requirements. The achieved resolution performance must be consistent with an appropriately defined resolution budget.

2.7.2 Element 2 – Readout

2.7.2.1 TRL 4 Element 2.1—Microwave SQUID Multiplexing

Milestone TRL 4-2.1 — Design and fabricate microwave SQUID circuitry with the appropriate noise level and resonator bandwidths and resonance frequency spacing for the LXM microcalorimeters.

Significance—Microwave SQUID multiplexing demonstrations exist that achieved the appropriate noise levels, but at (1) lower slew rates with the appropriate resonance frequency spacing or (2) higher

slew rates but larger spacing. To achieve the appropriate noise level at the slew rates required to read out the hydras requires a separate optimization of resonator bandwidth for each of the three LXM pixel types. The chain of optimizations is (1) a target current noise determines an input coupling, (2) a target slew rate determines a flux-ramp repetition rate, (3) the flux-ramp rate determines resonator bandwidth, and (4) a crosstalk requirement determines the spacing between resonances, and therefore the number of channels that can be multiplexed on a single line.

Verification—Verify that the microwave SQUID circuits agree with design parameters within a factor of 2. Read out prototype LXM arrays using the microwave SQUID circuits. Demonstrate that the bandwidths shown in Table 6 are sufficient to meet the LXM detector system performance requirements.

Milestone TRL 4-2.2 — Demonstrate readout of the relevant pixel types at reduced multiplexing factors with energy resolution degradation from the readout of less than 30% of single-pixel readout.

Significance—Not attempting to reach the full multiplexing factor in this step minimizes design and fabrication time while still providing abundant information on interactions between the sensor and readout systems. At reduced multiplexing factors, the channel-to-channel direct crosstalk can be carefully compared to model predictions.

Verification—Read out prototype LXM arrays using the microwave SQUID circuits. Measure the energy resolution and confirm it is degraded by no more than 30% compared to single-pixel readout.

Milestone TRL 4-2.3 — Demonstrate readout of relevant pixel types with energy resolution degradation from the readout of <30% of single-pixel readout at relevant multiplexing factors.

Significance—This milestone will demonstrate control of the resonator frequency and bandwidth such that relevant numbers of resonators can be fabricated and tested without frequency collisions or significant crosstalk. At relevant multiplexing factors, the crosstalk conditions should be similar to the crosstalk conditions of the LXM and allow validation of the models (100 resonators for the Main Array and Ultra-Hi-Res Array and 10 resonators for the Enhanced Main Array are expected in the demonstration).

Verification—Read out prototype LXM arrays using the microwave SQUID circuits. Measure the energy resolution and confirm it is degraded by no more than 30% compared to single pixel readout.

Milestone TRL 4-2.11 — For MMC readout, demonstrate sufficiently low coupled energy sensitivity, high enough input inductance, and reduced lithographic area per SQUID to enable the readout of MMCs with <30% degradation of energy resolution compared with single-pixel readout.

Significance—MMCs require lower-noise microwave SQUID resonators in order to optimize their energy resolution. They also require higher inductance input coils in order for the MMC input circuit to be optimized by minimizing the effects of stray inductance, and low areas of SQUID resonators to minimize the size of readout chips.

Verification—Read out prototype LXM MMC arrays using the microwave SQUID circuits. Measure the energy resolution and confirm it is degraded by no more than 30% compared to single-pixel readout.

2.7.2.2 TRL 5 Element 2.1—Microwave SQUID Multiplexing

Milestone TRL 5-2.1 — Demonstrate readout of all relevant pixel types at required multiplexing

factors across the full bandwidth with energy resolution within the error budget allocation.

Significance—This milestone will demonstrate that the required resonator density can be achieved across the full readout bandwidth without energy degradation for relevant pixel types. Achieving the full 4–8 GHz bandwidth will require that multiple resonator chips be connected in series without significant impedance discontinuities from chip-to-chip connections. It will also require successful integration with a representative amplifier chain.

Verification—Read out prototype LXM arrays using the microwave SQUID circuits. Measure the energy resolution and confirm it meets the error budget allocation.

Milestone TRL 5-2.2 — Demonstrate microwave SQUID multiplexer circuit performance is not degraded by more than allocated by the error budget for radiation dose equivalent to 5 years at L2.

Significance—This demonstration is required to confirm that LXM will meet the observation efficiency and lifetime requirements.

Verification—Measure circuit performance before and after 5-year-equivalent dose and assess changes in resonator characteristics. Confirm that any damage or excess noise is within the error budget allocation.

2.7.2.3 TRL 6 Element 2.1—Microwave SQUID Multiplexing

Milestone TRL 6-2.1 — Demonstrate a scalable readout geometry and test at least one quarter of the pixels simultaneously to demonstrate that they meet the readout performance requirements. The yield of functioning readout for pixels meeting all noise and input slew rate requirements is >95%.

Significance—This milestone will demonstrate that a scalable readout has been developed with sufficient yield of low-temperature components and sufficiently low crosstalk between pixels/channels that the readout is ready to be developed for a flight program. It will also require successful integration with a representative amplifier chain.

Verification—Read out at least one quarter of the prototype TRL 6 LXM array using the microwave SQUID circuits. Measure the energy resolution and confirm that the fraction of pixels meets the readout error budget allocation of >95%.

2.7.2.4 TRL 4 Element 2.1 – Code-Division Multiplexing (BACKUP APPROACH)

Milestone TRL 4-2.4 — Demonstrate CDM circuitry that provides appropriate noise, switching speeds, input channel count, and circuit yield.

Significance—This confirms that CDM meets the component-level requirements prior to integrating with a detector array.

Verification—Characterize the CDM circuitry and confirm that the parameters are consistent with model predictions within a factor of two.

Milestone TRL 4-2.5 — Demonstrate readout of the relevant pixel types using CDM integrated with an error correction capability.

Significance—An essential step toward confirming that the CDM design and fabrication is suitable for LXM. Error correction capability would allow recovery from scenarios where a single SQUID fails (e.g., due to static discharge or radiation damage) and the demodulation matrix becomes under-constrained and information for the entire column of TESs is lost. Error correction should be demonstrated that avoids degradation.

Verification—Read out prototype LXM arrays using CDM. Measure the energy resolution and confirm that any energy resolution degradation is consistent with model predictions.

Milestone TRL 4-2.6 — Demonstrate readout of relevant pixel types at relevant multiplexing factors using CDM.

Significance—Confirm that the CDM design and fabrication is suitable for LXM.

Verification—Read out prototype LXM arrays using CDM at relevant multiplexing factors. Measure the energy resolution and confirm that any energy resolution degradation is consistent with model predictions.

2.7.2.5 TRL 5 Element 2.1—Code-Division Multiplexing (BACKUP APPROACH)

Milestone TRL 5-2.3 — Demonstrate CDM circuit performance is not degraded by more than allocated by the resolution budget for radiation doses equivalent to 5 years at L2.

Significance—This demonstration is required to confirm that the LXM will meet the observation efficiency and lifetime requirements (if using this backup readout option).

Verification—Measure circuit performance before and after 5-year equivalent dose and assess changes in circuit characteristics. Confirm that any damage or excess noise is within the error budget allocation.

Milestone TRL 5-2.4 — Demonstrate readout of required pixel types at a representative number of columns with energy resolution degradation within error budget allocation.

Significance—A large number of columns will be needed to read out the required number of microcalorimeters for LXM. Advancing from TRL 4 to 5 will require engineering improvements, including demonstrations that fabrication process can provide the necessary yield and uniformity.

Verification—Read out prototype LXM arrays using CDM at relevant multiplexing factors. Measure the energy resolution and confirm it meets the error budget allocation.

2.7.2.6 TRL 4 Element 2.2—HEMT Amplifiers

Milestone TRL 4-2.7 — Analyze HEMT architecture and identify the production path and a path to produce flight-qualified HEMTs.

Significance—The semiconductor amplifier, known as an HEMT, which amplifies the microwave tones in microwave SQUID readouts, plays an important role in determining noise, bandwidth, and crosstalk in the readout chain. Signals are carried into and out of the HEMT using coaxial or metal-on-Kapton cabling. Commercial HEMT amplifiers exist with excellent properties, but *Lynx* may benefit from (or require) HEMTs with different design optimizations. The power dissipation of individual HEMTs is on the order of 1 mW, and as many as 16 HEMTs may be on at a time, so the HEMTs will have a significant effect on the thermal budget of the mission.

Verification—Analyze HEMT architecture, i.e., study the number of stages needed, thermal locations of stages, gain/stage, noise/stage, power/stage, linearity/stage, and connections between stages. Identify the production path (commercial, custom, and mix of commercial and custom) and a path to produce flight-qualified HEMTs.

Milestone TRL 4-2.8 — Demonstration of HEMT architecture (a single HEMT amplifier).

Significance—This step consists of demonstrating an optimized HEMT with noise, gain, and

linearity that meet specifications while simultaneously demonstrating the predicted power dissipation.

Verification—Characterize the HEMT noise, gain, and linearity, and confirm that it agrees with the predicted values. Measure the power dissipation and confirm that it does not exceed its thermal budget.

2.7.2.7 TRL 5 Element 2.2—HEMT Amplifiers

Milestone TRL 5-2.5 — Demonstrate HEMT architecture and appropriate cabling (three or more HEMTs in a flight-like configuration, each connected to appropriate cabling).

Significance—The crosstalk between separate microwave signal chains (each with a single HEMT) is expected to be low, but this must be measured and verified using the appropriate configuration and cabling prior to the full-scale FPA demonstration.

Verification—Confirm that the level of crosstalk between output channels with separate HEMTs is consistent with the error budget.

2.7.2.8 TRL 4 Element 2.3—Readout Electronics

Milestone TRL 4-2.9 — Assemble appropriate room temperature readout electronics using commercial parts as a breadboard model spanning a bandwidth of 1–2 GHz (these electronics do not need to be coupled to low-temperature readout components).

Significance—It is a system built using a Commercial Off-the-Shelf (COTS) FPGA evaluation board, ZCU102, which has UltraScale+ MPSoC ZU9EG, a lower-grade version of the same family proposed in the readout that will be flight-qualified. For the ADCs and DACs, a COTS daughterboard that is mountable onto the FPGA board can be used. With fewer resources available in this FPGA compared to the one envisaged for use on LXM, it may not be possible to implement a full readout system for the entire 4-GHz bandwidth of a HEMT. However, it would be practical to implement a complete readout system for a 1–2 GHz sub-band.

Verification—Confirm that the readout electronics perform as expected.

Milestone TRL 4-2.10 — With the COTS room temperature electronics (described previously), demonstrate readout of relevant pixel types at relevant multiplexing factors over a 1- to 2-GHz bandwidth using microwave SQUID multiplexer components.

Significance—This configuration allows a check of the resource usage and power dissipation in the FPGA and an accurate estimate of the total required resources and power dissipation of the LXM room temperature readout system.

Verification—Measure the resource usage and power dissipation in the FPGA and confirm that it agrees with model predictions.

2.7.2.9 TRL 5 Element 2.3—Readout Electronics

Milestone TRL 5-2.6 — Assemble room temperature readout electronics as a brassboard model using flight-qualified parts, or non-flight parts when flight-qualified versions of the parts exist or are undergoing the NASA space qualification process.

Significance—This milestone proves that a suitable room temperature readout electronics system may be built using parts. A system with at least 1–2 PCBs for each module (e.g., the signal processing boards with FPGA and ADC/DAC, the power modules, and the RF modules) would be sufficient as

long as it can read out at least two HEMTs simultaneously. It is crucial that all the parts in the system have flight qualified versions or are undergoing the NASA space qualification process. The FPGA, ADC, and DAC are highly likely to all be flight qualified at this point, but RF components, such as amplifiers, mixers, and oscillators may still be undergoing the NASA space qualification process.

Verification—Confirm that the readout electronics system performs as expected and is consistent with the results predicted based on measurements of the TRL 4 system using COTS parts.

Milestone TRL 5-2.7 — Demonstrate isolated readout of relevant pixel types at relevant multiplexing factors at frequencies ranging over the full range of bandwidth of the HEMT (typically 4 GHz) using a room temperature readout electronics system built with flight-qualified parts, or non-flight parts when flight-qualified versions of the parts exist or are undergoing the NASA space qualification process.

Significance—This milestone confirms that the readout electronics system meets performance requirements, but does not demonstrate critical scaling requirements.

Verification—Measure pixel energy resolution and verify that any degradation caused by the readout system is compatible with the error budget allocation. Confirm that the electronics system is able to perform adequately at selected frequencies across the bandwidth of the HEMT.

Milestone TRL 5-2.8 — Demonstrate simultaneous readouts of relevant pixel types at relevant multiplexing factors over a full range of bandwidth of more than two HEMT channels (typically 4 GHz per HEMT) using a room temperature readout electronics system built with flight-qualified parts, or non-flight parts when flight-qualified versions of the parts exist or are undergoing the NASA space qualification process.

Significance—This milestone confirms that the readout electronics system meets performance requirements when operating all pixels coupled to resonators spread across a bandwidth of more than two HEMT channels.

Verification—Measure pixel energy resolution and verify that any degradation caused by the readout system is compatible with the error budget allocation. Confirm that the electronics system performs adequately during this simultaneous operation across the required bandwidth.

Milestone TRL 5-2.9 — Demonstrate that the heatsinking between the PCB and chassis is adequate to dissipate the heat generated from the high-power components (FPGA, ADC, and DAC).

Significance—The heatsinking must be demonstrated to ensure that the junction temperatures of the FPGAs, DACs, and ADCs remain within requirements. If the heatsinking is not adequate, modifications such as increasing the thermal conductance (adding metal) or increasing the number of FPGAs to distribute the load and reduce the power dissipation in a single FPGA may be required.

Verification—Measure temperatures at relevant locations and calculate the relevant thermal conductances. Confirm that the results agree with the requirements of the thermal model.

Milestone TRL 5-2.10 — Develop Board Support Equipment (BSE) / Ground Support Equipment (GSE) for a signal emulator to emulate the cold electronics and test the developed system to ensure the system meets the full requirements.

Significance—The system can be designed as a modular system using Xilinx UltraScale+™ RFSoC FPGA so that it can be diverted into the signal processing board when RFSoC becomes available for flights.

Verification—Generate and measure signals using the BSE/GSE and confirm that the system can adequately reproduce the signals expected from the cold electronics (e.g., signal shape, noise content).

2.7.2.10 TRL 6 Element 2.3—Readout Electronics

Milestone TRL 6-2.2 — A full-scale readout system for at least one quarter of the array needs to be designed, constructed, and tested using flight-qualified parts, or non-flight parts when flight-qualified versions of the parts exist. This system should be assembled in a realistic form factor.

Significance—This demonstration meets the TRL 6 requirements of a high-fidelity system prototype.

Verification—Verify that that the system can read out the requisite number and type of microcalorimeter pixels with performance consistent with the error budget allocations. Confirm that system meets the required power and thermal requirements.

2.7.3 Element 3—Focal Plane Assembly and Filters

2.7.3.1 TRL 5 Element 3.1—Mechanical Design and Magnetic Shielding

Milestone TRL 5-3.1 — Determine kinematic mounting approaches for the Main Array and the anticoincidence detector, and the microwave SQUID resonator chips together with Nyquist inductors and bias resistors.

Significance—This is required to verify that the mounting approaches used in previous microcalorimeter instruments can be adapted for LXM.

Verification—Simulate design and verify it meets requirements related to launch loads. Design and build prototypes.

Milestone TRL 5-3.2 — Perform simulations and experiments to determine whether there will be issues related to RF signals interfering with each other among the different microwave SQUID resonator chips. Demonstrate readout of all relevant pixel types at required multiplexing factors with energy resolution within the error budget allocation.

Significance—Separate small metal housings for each microwave chip may be needed, which would significantly affect the mechanical design of the FPA. The outcome of this study will determine the size of microwave resonator chips that are mounted to the eight sides of the octagonal FPA and any additional RF shielding needed within the FPA.

Verification—Build prototype and test to verify that the level of interference is low. Confirm that the level of interference agrees with the model to within a factor of 2.

Milestone TRL 5-3.3 — Verify the thermal and mechanical properties of the T-300 cone-shaped thrust tubes used for mechanical support of the FPA between different temperature stages and verify the mechanical properties and the DC- and AC-shielding performance of the magnetic shields.

Significance—The current approach planned for the mechanical mounting of the FPA and all the different components at 50 mK and 600 mK assumes the use of thin, T-300 (carbon-fiber-reinforced polyimide) cone-shaped thrust tubes between the different temperature stages. The assumed mechanical and thermal properties must be verified to meet LXM requirements. Mu-metal and superconducting magnetic shields similar to those in development for the *Athena* X-IFU will

be used to provide magnetic shielding of the microcalorimeter array and the readout circuits. These must be built and tested to validate the FPA design.

Verification—Measure the mechanical and thermal properties of T-300 thrust tubes with appropriate form factors and at relevant temperatures; verify that the results are consistent with the LXM mechanical and thermal system requirements. Confirm that the level of magnetic shielding is greater than or equal to that required for the LXM detectors and readout, and that the mechanical properties are consistent with simulations.

2.7.3.2 TRL 6 Element 3.1—Mechanical Design and Magnetic Shielding

Milestone TRL 6-3.1 — Design, build, and test a full-scale demonstration model FPA attached to a continuous ADR to provide representative temperatures/conditions for FPA operation. This will include appropriate interconnects (Element 3.2) and bump bonding (Element 3.3).

Significance—This will validate the FPA and interface designs.

Verification—Measure the temperatures (and temperature stability) at the various parts of the FPA over many continuous ADR cycles. Verify that the temperatures agree with predictions and that the temperature stability meets LXM requirements.

2.7.3.3 TRL 5 Element 3.2—Interconnects

Milestone TRL 5-3.4— Calculate appropriate coaxial cable design (lengths) needed for the stages at 4.5 K and below given known thermal conductance and mechanical properties, as well as the relevant LXM requirements. Design superconducting flex for the around-the-corner wiring between the sensor arrays and the microwave SQUID multiplexer (with number of traces appropriate for LXM). Build appropriate cables and measure thermal, mechanical, and electrical properties.

Significance—It is likely that connectorized coax cables that are suitable in size and thermal conductance for the LXM FP will be used between each HEMT and the readout at 50 mK. Currently, there are only limited data available on the properties of such interconnects. Measurements must be made to verify that the thermal and mechanical properties are suitable. The superconducting flex (around-the-corner wiring) is needed to carry signals between the detector arrays and the multiplexer chips. Measurements must be made to verify that the thermal, mechanical, and electrical properties are suitable for LXM.

Verification—Verify that measured values agree with predicted values. Verify that the components are mechanically robust with respect to launch loads.

2.7.3.4 TRL 6 Element 3.4—Infrared/Optical Blocking Filters

Milestone TRL 6-3.2 — Build a set of filters compatible with the FPA and cryostat design, including with appropriate kinematic mounts. Demonstrate in the relevant environments using a vibration table for mechanical verification and deployment in a cryostat to demonstrate thermal and magnetic shielding requirements.

Significance—The blocking filters are very fragile, and it is imperative to verify that the components survive vibration without damage to the thin films or support meshes. It is essential to verify that the system-level thermal requirements are met to confirm the validity of the mounting scheme and the performance of the filters in a relevant environment.

Verification—Perform detailed pre- and post-vibration inspections of each filter and verify that

the vibration did not cause any damage. Verify that the heat loads in the cryostat are compatible with those expected.

2.7.4 Element 4—Cryogenics

2.7.4.1 TRL 6 Element 4.1—Cryostat

Milestone TRL 6-4.1 — Design a cryostat that meets the thermal and structural requirements of LXM. Perform structural and/or thermal sample tests where suitable data for specific materials used in the design do not currently exist. (Note that right now LXM anticipates using materials with known properties.)

Significance—The LXM cryostat, which houses all components lower than room temperature, is based on design principles for many previously flown cryostats. The design challenge is primarily a tradeoff between structural and thermal performance and is considered normal engineering work for experienced cryogenic engineers. Previous missions employing long-life dewars operating at this low temperature include *IRAS*, *COBE*, *ISO*, *Suzaku*, *Hitomi*, *Spitzer*, and *Herschel*, among others. In the case of LXM, there will be no liquid helium, which simplifies the design. Nevertheless, the cryostat is considered TRL 5, and this milestone advances the LXM cryostat to TRL 6.

Verification—Verify that the design meets the thermal and structural requirements.

2.7.4.2 TRL 5 Element 4.2—Cryocooler (Pulse Tube Cryocooler)

Milestone TRL 5-4.1 — Design, fabricate, and demonstrate pulse tube cryocooler system with breadboard electronics using flight-compatible electronics components and verify that the system meets performance requirements and is compatible with expected launch loads.

Significance—Verifies pulse tube cryocooler design.

Verification—Verify that performance is consistent with requirements, including when using higher compressor power. Complete environmental testing and revalidate performance.

2.7.4.3 TRL 6 Element 4.2—Cryocooler (Pulse Tube Cryocooler)

Milestone TRL 6-4.2 — Demonstrate entire flight-like system performance pre- and post-launch loads environment. This demonstration includes flight-like electronics.

Significance—Verifies pulse tube cryocooler system design, including flight-like electronics.

Verification—Build system and verify that performance is consistent with requirements, including when using higher compressor power. Complete environmental testing and re-validate performance.

2.7.4.4 TRL 4 Element 4.2—Cryocooler (Reverse-Brayton Cryocooler)

Milestone TRL 4-4.1 — Demonstrate 4.5-K Reverse-Brayton cryocooler system-level performance in a laboratory environment (SBIR Phase II ongoing).

Significance—The great advantage of this type of cryocooler is the inherent lack of vibration generated by the cryocooler, as it is based upon the use of extremely low-mass moving parts moving at speeds in excess of 1 kHz, as well as the high mechanical reliability from the use of gas bearings and clearance seals that prevent mechanical contact and thus eliminate wear. It is also more thermodynamically efficient due to extraction of work by the cold turbo-alternators. This leads to

lower input power for the same cooling power. Its operation is completely independent of gravity. The drawback, however, is that it is currently at TRL 3. Although most components are at TRL 4–6, the 4.5-K stage remains to be demonstrated. Its development is currently based upon an existing 10-K cryocooler and a 4-K cooler under development for the U.S. Navy. The net refrigeration (gross refrigeration less parasitic losses) of the cryocooler is 89 mW at 4.5 K, 490 mW at 25 K, and 4.1 W at 75 K. This cryocooler requires <350 W from the spacecraft bus. The extremely high thermodynamic performance is inherent to the Brayton cycle at low temperatures. The mass of the cryocooler is 39 kg (29 kg for the mechanical cooler, 8 kg for 2 redundant sets of electronics, and 1.7 kg for a cross-strap box).

Although a 2-stage version of this cryocooler providing 236 mW of cooling at 10 K has been demonstrated, a version with a third stage of cooling to reach 4.5 K has been proposed for the LXM, and this is still in development under a NASA SBIR contract. Once the turbo-alternator is developed, a high-performance, low-temperature turbo-Brayton cryocooler can be assembled with low technical risk.

Verification—Verify performance is consistent with the LXM requirements.

2.7.4.5 TRL 5 Element 4.2—Cryocooler (Reverse-Brayton Cryocooler)

Milestone TRL 5-4.2 — Design system with appropriate support structure and perform vibration testing and post-vibration performance testing to demonstrate survival of launch loads for the 4.5 K Reverse-Brayton cryocooler system.

Significance—Confirms that the Reverse-Brayton cryocooler design is compatible with launch loads.

Verification—Assess pre- and post-vibration performance and verify that vibration did not cause damage or performance degradation.

2.7.4.6 TRL 6 Element 4.2 – Cryocooler (Reverse-Brayton Cryocooler)

Milestone TRL 6-4.3 — Demonstrate full system and perform environmental testing, including tests of the electronics. The design must be compatible with LXM mechanical requirements (for example, fit within the cryostat housing).

Significance—Confirms that the Reverse-Brayton cryocooler system meets LXM requirements and is compatible with launch loads.

Verification—Assess performance and confirm.

2.7.4.7 TRL 5 Element 4.3—Continuous ADR (Sub-Kelvin Cooler)

Milestone TRL 5-4.3 — Demonstrate performance and meeting of launch load vibrational requirements. Verify sufficient reliability of all ADR heat switches, and salt pill suspensions within the CADR. Verify low external magnetic field (<30 μT).

Significance—To raise the 50-mK CADR to TRL 5 requires adding to the system and demonstrating a high-performance magnetic shield, as well as the demonstration of meeting launch load vibrational requirements. These steps are in progress as part of a Research Opportunities in Space and Earth Sciences (ROSES) SAT program that is taking place at GSFC within the cryogenics group. This project will be completed by the end of CY19, and result in a sub-Kelvin cooler at TRL 5, required to meet the LXM requirements.

Verification—Verify pre- and post-vibration performance meets requirements, and confirm that the ADR heat switches are sufficiently reliable.

2.7.4.8 TRL 6 Element 4.3—Continuous ADR (Sub-Kelvin Cooler)

Milestone TRL 6-4.4 — Verify complete 5-stage design including 0.6-K continuous stage and demonstrate full system performance (including flight-like electronics) meets LXM requirements.

Significance—To advance this CADR to TRL 6, a secondary continuous stage operating at 0.6 K must be added. This is a straightforward addition of another stage and its support and heat switch. Note that the flight electronics boards for the CADR control have previously flown on *Hitomi* and will be flown on *XRISM*. Only the controller housing will be resized to accommodate the LXM CADRs board count (7 boards rather than 5 on *Hitomi*).

Verification—Verify performance meets LXM requirements.

Milestone TRL 6-4.5 — Demonstrate 6-mW cooling at 50 mK. Increase size of components of the CADR and increase suspension strength and stiffness. Perform launch loads testing and verify performance.

Significance—The TRL 5 demonstration will not have the requisite cooling power at 50 mK; in order to increase to TRL 6, the required 6-mW cooling at 50 mK must be demonstrated.

Verification—Verify performance before and after launch loads testing.

2.8 TRL Development Schedule

The model philosophy of the LXM is based upon the approach that was followed by the SXS instrument on *Astro-H* and is similar to the approach planned for the *Athena* X-IFU. It is based on the development of an engineering model and a protoflight unit, with selected subsystem flight spares but no complete instrument spare. There is no qualification model at the instrument or subsystem level (as is planned for the X-IFU), but it is planned that the engineering model will undergo extensive qualification testing beyond the typical level of an engineering development unit in order to space-qualify the design.

What is important to the success of the schedule is that the detectors and readout components begin work towards the engineering model and flight model prior to the overall instrument PDR and Critical Design Review (CDR), respectively, following Key Decision Point (KDP) reviews for just these two items. This is due to the long lead times associated with the design, fabrication, and testing of these components, which must all be complete prior to integration and testing within the FPA. The FPA, in turn, needs to be integrated and tested with the rest of the instrument. The long sequence typically consists of approximately a year of development to produce the detector, and another year to integrate and test within the FPA. In order to address the lessons learned from the engineering model development, it is critical that the flight model does not begin until the engineering model FPA has been tested, and ideally after all tests on the engineering model are complete. For this to happen, in order to align it with the development schedule for the rest of LXM and the rest of the mission, the detectors and readout should be at TRL 6 by the end of Phase A (September 30, 2026). Our development plan achieves this with 9 months of margin.

Fig. 19 shows the LXM schedule for technology development from March 2019 through pre-Phase A and Phase A, and shows how:

1. All the critical technologies needed for LXM will achieve TRL 4 by the start of pre-Phase A, funded through ongoing existing research and development programs. (As noted in earlier sections, it is likely that via these ongoing programs LXM will achieve TRL 4 significantly earlier. The baseline (TES) sensor detectors will reach TRL 4 by December 31, 2019, and the baseline (μMUX) readout likely by December 31, 2020, although development of parallel technology options reaching TRL 4 will continue through December 2, 2021.)
2. All the critical technologies that are baselined will achieve TRL 5 prior to the end of pre-Phase A, with 9 months of margin.
3. The critical detector and readout technologies will achieve TRL 6 by the end of Phase A through a TRL 6 Demonstration Unit, with 7 months of margin.

From a schedule perspective, the LXM will benefit greatly from the availability of additional experienced engineers and scientists becoming available during Phase A to complement the LXM development team following the launch and commissioning of *XRISM*, and from the ramp-down of *Athena* X-IFU activities during Phase B. From this perspective, the schedule for the development of the LXM is ideal.

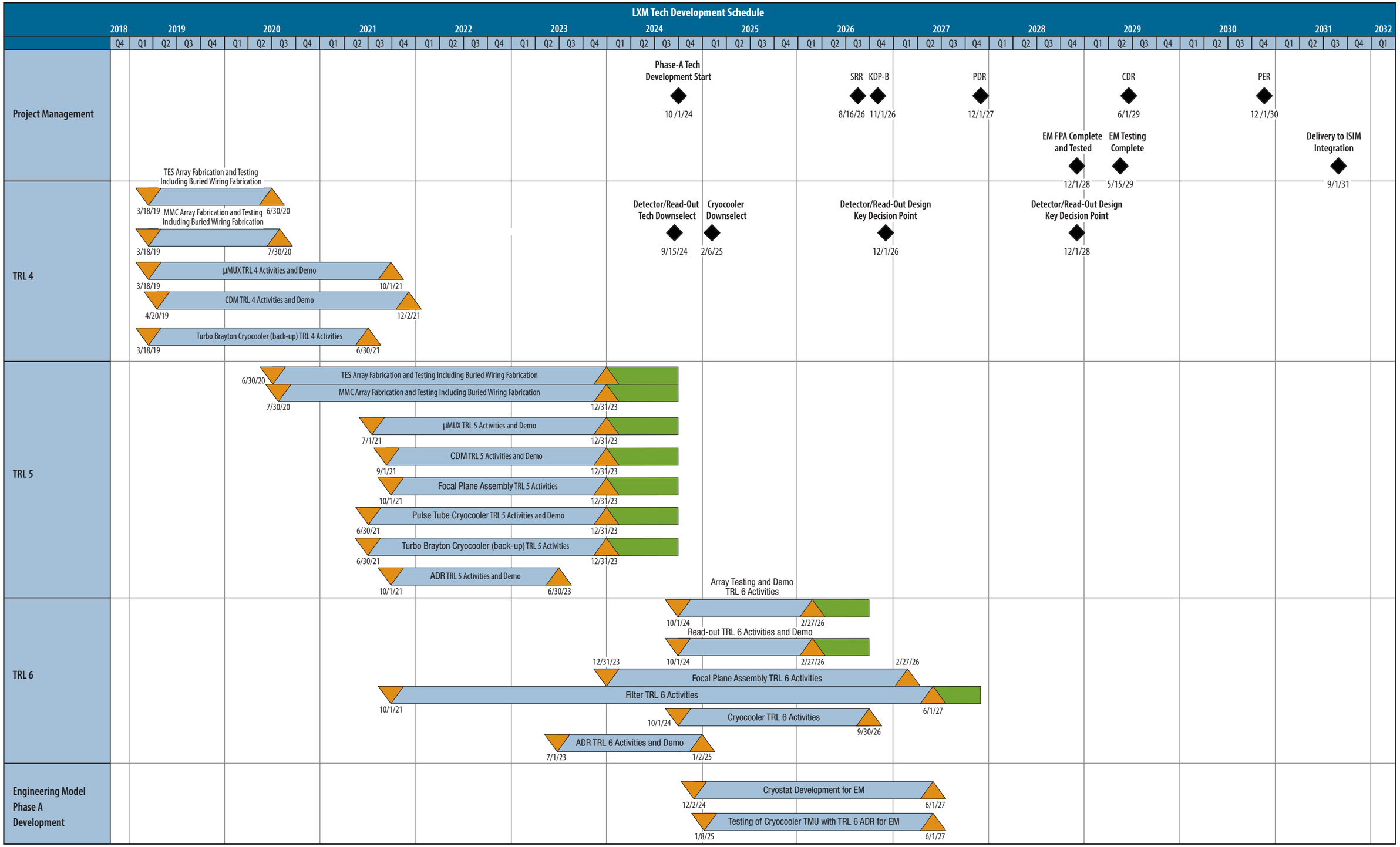

Fig. 19—LXM technology development schedule.

2.9 Cost

Redacted

2.10 Risks

The subsections below identify risks for the LXM, broken out by the various technologies. Detector risks are provided first, followed by microwave readout, FPA and filters, and cryogenics risks.

Table 8—Summary of LXM maturation risks.

Risk	Title	L	C	T	S	$
LXM-1(a)	Non-linearity of detectors with energy makes energy resolution/discrimination harder	3	3	X	X	X
LXM-1(b)	Inability to reduce the slew rates for the hydra pixels to match readout	2	2	X	X	X
LXM-2	Unable to fabricate desired heatsinking of arrays with buried wires is difficult to achieve	2	3	X	X	X
LXM-3	Uniformity of performance is not sufficient to meet *Lynx* requirements	1	2	X	X	X
LXM-4	Meeting the target readout noise level	1	3	X	X	X
LXM-5	Resolution degradation from crosstalk	2	3	X	X	X
LXM-6	Frequency collisions from the large number of resonators	3	2	X	X	X
LXM-7	Radiation damage of microwave SQUID multiplexer	1	3	X	X	X
LXM-8	Reduced signal to noise due to reflections off of impedance discontinuities	2	2	X	X	X
LXM-9	Failure to achieve an optimal HEMT amplifier design	1	3	X	X	X
LXM-10	Failing to meet the target HEMT noise, gain, and linearity specifications, while simultaneously achieving the target power dissipation	1	2	X	X	X
LXM-11	RF signals interfere with one another on the different microwave SQUID resonator chips when mounted in a flight-like configuration	2	2	X	X	X
LXM-12	Bump bonding is non-reversible process	1	2	X	X	X
LXM-13	Thin-film filters are damaged during handling, cryogenic operation, or during environmental testing	2	1	X	X	X
LXM-14	Cryocooler does not reach TRL 5 by Phase A	2	3	X	X	X
LXM-15	CADR does not reach TRL 5 by Phase A	1	1	X	X	X

L = likelihood of occurrence; C = consequence; T = technical risk, S = schedule risk, $ = cost risk

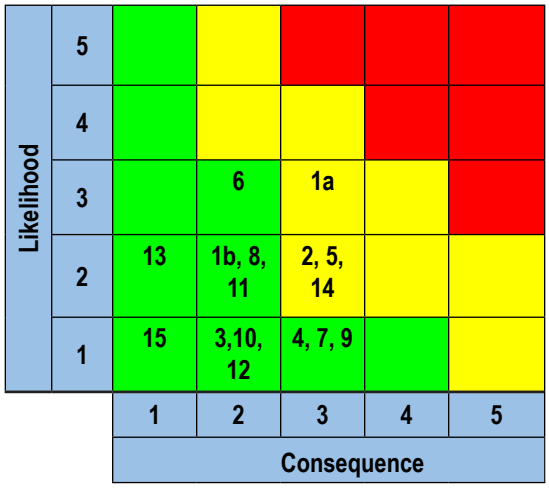

Fig. 20—LXM detector risk ranking.

Risk LXM-1 — It may not be straightforward to achieve the desired energy resolution and position discrimination at all energies for the specified rise and fall times. Although the desired performance goals for TRL 4 are feasible, there is risk that non-linearity in TES detectors with energy, and the ability to adequately reduce the slew rates for the hydra pixels to match the readout capabilities of the microwave multiplexing, will not be demonstrated.

Mitigation—There is a planned parallel development of a second sensor technology, MMCs, as well as the baseline TES technology. The inherently more linear energy scale of the MMCs and their higher intrinsic heat capacity offer additional design flexibility to adjust the thermal design of the hydras to meet the required specifications. Alternative mitigation options are reducing the count rate requirement or the number of pixels in a hydra. This latter option reduces the slew rate of the fastest pixel, making them easier to read out at the expense of requiring more sensors and resonators in the FPA, and possibly more HEMTs.

Risk LXM-2 — Fabrication of desired heatsinking of arrays with buried wires in order to sufficiently reduce thermal crosstalk is difficult to achieve.

Mitigation—Multiple heatsinking approaches are in development for TESs and MMCs. These include the use of gold heatsink layers on the top surface of the detector substrate, as well as the bottom surface.

Risk LXM-3 — Uniformity of performance is not sufficient to meet *Lynx* requirements.

Mitigation—Use of TES sensor designs with very little contact between the TES bilayer and normal metal features will be the prioritized, which has been shown to reduce non-uniformities. In addition, the MMC backup is inherently more uniform.

Risk LXM-4 — Meeting the target readout noise level.

Mitigation—Proper design of the input coupling strength, understanding and optimizing the noise contributions of the semiconductor amplifier and two-level systems, and implementation of spread-spectrum input coupling techniques.

Risk LXM-5 — At relevant μMUX factors, another major risk is energy resolution degradation from crosstalk, which can originate from low-frequency coupling between sensor circuits, high-frequency coupling within the resonator and feedline circuitry, and non-linearities in the common readout elements, especially the semiconductor amplifier.

Mitigation—Crosstalk can be mitigated in a variety of ways, including careful design of the amplifier (usually called a HEMT), careful design of the RF-SQUID and resonator circuitry, operation at lower tone powers, and applying feedback to the tone frequencies (tone tracking) to reduce the power seen by the HEMT.

Risk LXM-6 — Frequency collisions from the large number of resonators and the integration of the resonators into the folded focal plane architecture.

Mitigation—The risk of frequency collisions can be mitigated by good fabrication process control and post-fabrication adjustment of resonator properties.

Risk LXM-7 — Radiation damage of microwave SQUID multiplexer.

Mitigation—This risk is mitigated by studies of possible mechanisms of degradation and early

integration into the multiplexer circuit design of strategies to reduce the impact of damage or recover from the damage by shifting the probe frequencies.

Risk LXM-8 — Reduced signal-to-noise due to reflections off of impedance discontinuities from the connections required to integrate all of the required circuitry into the folded focal plane architecture.

Mitigation—This risk can be mitigated by careful testing of all components and interconnect strategies at early stages of the component design process. Also, isolation components such as compact circulators and directional couplers could be further integrated in the design.

Risk LXM-9 — Failure to achieve an optimal HEMT amplifier design because of imperfect understanding of the design trade space. For example, a better understanding is needed of noise versus physical temperature.

Mitigation—A combination of experimental work, first-principles knowledge building, and closer interaction with existing HEMT designers and vendors.

Risk LXM-10 — Failing to meet the target HEMT noise, gain, and linearity specifications while simultaneously achieving the target power dissipation.

Mitigation—HEMT properties can often be improved at the cost of higher dissipation. The risk can be mitigated by changes elsewhere in the readout that increase or decrease the microwave tone power reaching the HEMT. Risk can also be mitigated by changes in the mission cooling chain to better match available and dissipated powers.

Risk LXM-11 — Bump bonding is a irreversible process. While the plan to use bump bonding addresses the need to make a large number of interconnections, disassembly and replacing components will not be possible once the bump bonds are made. The entire assembly will become one high-value component.

Mitigation—Mitigation might include additional cost and schedule reserve.

Risk LXM-12 — There are issues related to RF signals interfering with each other among the different microwave SQUID resonator chips once they are mounted in a flight-like configuration, causing noise in excess of the energy resolution budget.

Mitigation—Design separate metal housings for each resonator chip to reduce the level of interference.

Risk LXM-13 — The thin-film filters are fragile. There is a risk that they will be damaged during handling, cryogenic operation, or during environmental testing.

Mitigation—Ensure robust processes are in place for handling, installation, operation, and environmental testing. Leverage experience in filter design and testing gained from the *Athena* X-IFU. If damage arises from a design issue, the alternate filter technology development provides risk mitigation. These lower-TRL waveguide-cutoff filters could eliminate the need for thin films on the inner filters (coldest stages) and allow thicker films on the outer filters.

Risk LXM-14 — Neither of the two cryocooler technologies reached TRL 5 by the start of Phase A, incurring more Phase A development cost and potential schedule delays.

Mitigation—There is a plan to have two cryocooler technologies fully developed in FY22 and FY23, with generous margin for reaching TRL 5.

Risk LXM-15 — The CADR does not meet all of its requirements for TRL 5 before Phase A, then more Phase A development costs will be incurred.

Mitigation—This development schedule is designed to be complete more than two years before the start of Phase A, but there exists two years of margin.

3 Summary

The roadmap for advancing the LXM detector and readout technologies from their current level of development to TRL 5 by the start of Phase A has 9 months of margin, and to TRL 6 by the end of Phase A has 7 months of schedule margin. Key milestones are identified. A development program has been designed to achieve these milestones. The main risks and the advancing level of difficulty have been assessed. While this is a complex instrument and a number of risks have been identified, almost all have a relatively low likelihood of occurring and the consequences are not major.

We have a high degree of confidence in the budget and schedule based upon the substantial experience the U.S. X-ray microcalorimeter teams have in developing instruments for *Astro-E*, *Astro-E2*, *Hitomi*, and more recently from the ongoing development of *XRISM* and the U.S. contribution to the *Athena* X-IFU. NASA has invested heavily in the development of TES and MMC detectors and their associated multiplexed readout for the past two decades. The U.S. teams lead the world in this area. The level of detail in this roadmap reflects the very high degree of knowledge and experience that exists with this technology, and the three recent major technological breakthroughs thighlighted in the introduction gives us confidence that the LXM technology development will proceed rapidly between now and the end of 2026.

4 Appendices

4.1 NASA TRL Definitions

TRL definitions per NPR 7123.1B, Appendix E, are reproduced in their entirety in Table 10.

Table 9—NASA TRL definitions.

TRL	Definition	Hardware Description	Software Description	Exit Criteria
1	Basic principles observed and reported	Scientific knowledge generated underpinning hardware technology concepts/applications.	Scientific knowledge generated underpinning hardware technology concepts/applications.	Peer reviewed publication of research underlying the proposed concept/application.
2	Technology concept and/or application formulated	Invention begins, practical applications is identified but is speculative, no experimental proof or detailed analysis is available to support the conjecture.	Practical application is identified but is speculative; no experimental proof or detailed analysis is available to support the conjecture. Basic properties of algorithms, representations, and concepts defined. Basic principles coded. Experiments performed with synthetic data.	Documented description of the application/concept that addresses feasibility and benefit.
3	Analytical and experimental critical function and/or characteristic proof-of- concept	Analytical studies place the technology in an appropriate context and laboratory demonstrations, modeling and simulation validate analytical prediction	Development of limited functionality to validate critical properties and predictions using non-integrated software components.	Documented analytical/ experimental results validating predictions of key parameters.
4	Component and/ or breadboard validation in laboratory environment	A low fidelity system/component breadboard is built and operated to demonstrate basic functionality and critical test environments, and associated performance predictions are defined relative to final operating environment.	Key, functionality critical software components are integrated and functionally validated to establish interoperability and begin architecture development. Relevant environments defined and performance in the environment predicted.	Documented test performance demonstrating agreement with analytical predictions. Documented definition of relevant environment
5	Component and/ or Breadboard validation in relevant environment.	A medium fidelity system/component brassboard is built and operated to demonstrate overall performance in a simulated operational environment with realistic support elements that demonstrate overall performance in critical areas. Performance predictions are made for subsequent development phases	End-to-end software: Elements implemented and interfaced with existing systems/simulations conforming to target environment. End-to-end software system tested in relevant environment, meeting predicted performance. Operational environment performance predicted. Prototype implementations developed.	Documented test performance demonstrating agreement with analytical predictions. Documented definition of scaling requirements
6	System/subsystem model or prototype demonstration in a relevant environment.	A high fidelity system/component prototype that adequately addresses all critical scaling issues is built and operated in a relevant environment to demonstrate operations under critical environmental conditions.	Prototype implementations of the software demonstrated on full-scale, realistic problems. Partially integrated with existing hardware/software systems. Limited documentation available. Engineering feasibility fully demonstrated.	Documented test performance demonstrating agreement with analytical predictions

TRL	Definition	Hardware Description	Software Description	Exit Criteria
7	System prototype demonstration in an operational environment.	A high fidelity engineering unit that adequately addresses all critical scaling issues is built and operated in a relevant environment to demonstrate performance in the actual operational environment and platform (ground, airborne, or space).	Prototype software exists having all key functionality available for demonstration and test. Well integrated with operational hardware/software systems demonstrating operational feasibility. Most software bugs removed. Limited documentation available.	Documented test performance demonstrating agreement with analytical predictions
8	Actual system completed and "flight qualified" through test and demonstration	The final product in its final configuration is successfully demonstrated through test and analysis for its intended operational environment and platform (ground, airborne, or space)	All software has been thoroughly debugged and fully integrated with all operational hardware and software systems. All user documentation, training documentation, and maintenance documentation completed. All functionality successfully demonstrated in simulated operational scenarios. Verification and Validation (V&V) completed.	Documented test performance verifying analytical predictions.
9	Actual system flight proven through successful mission operations.	The final product is successfully operated in an actual mission.	All software has been thoroughly debugged and fully integrated with all operational hardware and software systems. All documentation has been completed. Sustaining software support is in place. System has been successfully operated in the operational environment	Documented mission operational results.

4.2 AD^2 Definitions

AD^2 is a description of what is required to move a system, subsystem, or component from one TRL to the next. TRL is a static description of the current state of the technology as a whole. AD^2 is what it takes in terms of cost, schedule, and risk to advance to the next TRL. AD^2 is defined on a scale of 1–9 in a manner similar to TRL. The description of the AD^2 levels is shown in Table 11.

Table 10—AD^2 level definitions.

AD^2	Definition	Risk	Category	Success Chance
1	Exists with no or only minor modifications being required. A single development approach is adequate.	0%		Guaranteed Success
2	Exists but requires major modifications. A single development approach is adequate.	10%		
3	Requires new development well within the experience base. A single development approach is adequate.	20%		
4	Requires new development but similarity to existing experience is sufficient to warrant comparison across the board. A single development approach can be taken with a high degree of confidence for success.	30%	Well Understood (Variation)	Almost Certain Success
5	Requires new development but similarity to existing experience is sufficient to warrant comparison in all critical areas. Dual development approaches should be pursued to provide a high degree of confidence for success.	40%	Known Unknowns	Probably Will Succeed
6	Requires new development but similarity to existing experience is sufficient to warrant comparison on only a subset of critical areas. Dual development approaches should be pursued in order to achieve a moderate degree of confidence for success. Desired performance can be achieved in subsequent block upgrades with high confidence.	50%		
7	Requires new development but similarity to existing experience is sufficient to warrant comparison in only a subset of critical areas. Multiple development routes must be pursued.	70%		
8	Requires new development where similarity to existing experience base can be defined only in the broadest sense. Multiple development routes must be prepared.	80%	Unknown Unknowns	High Likelihood of Failure (High Reward)
9	Requires new development outside of any existing experience base. No viable approaches exist that can be pursued with any degree of confidence. Basic research in key areas needed before feasible approaches can be defined.	100%	Chaos	Almost Certain Failure (Very High Reward)

4.3 Risk Definitions

The standard risk scale for consequence and likelihood are taken from Goddard Procedural Requirements (GPR) 7120.4D, Risk Management Reporting. The definitions for likelihood and consequence categories are provided in Fig. 21.

Likelihood	Safety Estimated likelihood of Safety event occurrence	Technical Estimated likelihood of not meeting performance requirements	Cost Schedule Estimated likelihood of not meeting cost or schedule commitment
5 Very High	($P_{SE} > 10^{-1}$)	($P_T > 50\%$)	($P_{CS} > 75\%$)
4 High	($10^{-2} < P_{SE} \leq 10^{-1}$)	($25\% < P_T \leq 50\%$)	($50\% < P_{CS} \leq 75\%$)
3 Moderate	($10^{-3} < P_{SE} \leq 10^{-2}$)	($15\% < P_T \leq 25\%$)	($25\% < P_{CS} \leq 50\%$)
2 Low	($10^{-5} < P_{SE} \leq 10^{-3}$)	($2\% < P_T \leq 15\%$)	($10\% < P_{CS} \leq 25\%$)
1 Very Low	($10^{-6} < P_{SE} \leq 10^{-5}$)	($0.1\% < P_T \leq 2\%$)	($2\% < P_{CS} \leq 10\%$)

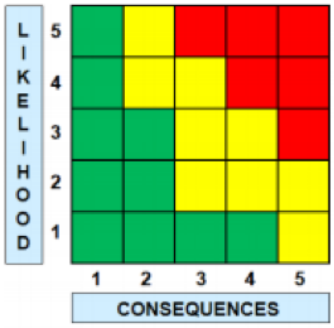

Consequence Categories					
Risk	**1 Very Low**	**2 Low**	**3 Moderate**	**4 High**	**5 Very High**
Safety	Negligible or not impact	Could cause the need for only minor first aid treatment	May cause minor injury or occupational illness or minor property damage	May cause severe injury or occupational illness or major property damage.	May cause death or permanently disabling injury or destruction of property.
Technical	No impact to full mission success criteria	Minor impact to full mission success criteria	Moderate impact to full mission success criteria. Minimum mission success criteria is achievable with margin	Major impact to full mission success criteria. Minimum mission success criteria is achievable	Minimum mission success criteria is not achievable
Schedule	Negligible or no schedule impact	Minor impact to schedule milestones; accommodates within reserves; no impact to critical path	Impact to schedule milestones; accommodates within reserves; moderate impact to critical path	Major impact to schedule milestones; major impact to critical path	Cannot meet schedule and program milestones
Cost	<2% increase over allocated and negligible impact on reserve	Between 2% and 5% increase over allocated and can handle with reserve	Between 5% and 7% increase over allocated and cannot handle with reserve	Between 7% and 10% increase over allocated, and/or exceeds proper reserves	>10% increase over allocated, and/or can't handle with reserves

HIGH RISK

MODERATE RISK

LOW RISK

Fig. 21—Risk matrix standard scale.

4.4 Acronyms

AD^2	Advancement Degree of Difficulty
ACTDP	Advanced Cryocooler Development Program
ADC	Analog to Digital Converter
ADR	Adiabatic Demagnetization Refrigerator
AGN	Active Galactic Nuclei
APRA	AstroPhysics Research and Analysis
CADR	Continuous ADR
CDM	Code-Division Multiplexing
CFRP	Carbon Fiber Reinforced Polyimide
DAC	Digital to Analog Converter
DC	Direct Current
DEEP	Digital Electronics and Event Processor
DUV	Deep Ultra-Violet
EDU	Engineering Development Unit
EM	Engineering Model
EMA	Enhanced Main Array
EMI	Electromagnetic Interference
FOV	Field or View
FPGA	Field Programmable Gate Array
FPA	Focal Plane Assembly
FWHM	Full Width at Half Maximum
GSFC	Goddard Space Flight Center
HEMT	High Electron Mobility Transistor
ISFM	Internal Scientist Funding Mode
IR	Infrared
JATIS	Journal of Astronomical Telescopes, Instruments, and Systems
JPL	Jet Propulsion Laboratory
LO	Local Oscillator
LXM	*Lynx* X-ray Microcalorimeter
MA	Main Array
MEB	Main Electronics Box
MIT/LL	Massachusetts Institute of Technology/Lincoln Laboratory
MMC	Metallic Magnetic Calorimeter
MXS	Modulated X-ray Source
MKIDs	Microwave kinetic Inductance Detectors
MUX	Multiplexer
NEP	Noise Equivalent Power
NIST	National Institute of Standards and Technology
PDR	Preliminary Design Review
RF	Radio Frequency
ROACH	Reconfigurable Open Architecture Computing Hardware
ROSES	Research Opportunities in Space and Earth Sciences
SAT	Strategic Astrophysics Technology

SOA	State of the Art
SLAC	Stanford Linear Accelerator Center
SQUID	Superconducting Quantum Interference Device
SNR	Supernova Remnant
STM	Structural-Thermal Model
TDM	Time Division Multiplexing
TES	Transition-Edge Sensor
TRL	Technology Readiness Level
UHR	Ultra-High-Resolution Array / Ultra-Hi-Res Array
UMUX	Microwave SQUID Multiplexer
UV	Ultra-Violet
X-IFU	X-ray Integral Field Unit
XRB	X-Ray Binary
XRISM	X-ray Imaging and Spectroscopy Mission

4.5 References

[1] [Bandler et al. 2019] S.R. Bandler et al., "The *Lynx* X-ray Microcalorimeter – LXM", Journal of Astronomical Telescopes, Instruments, and Systems 5(2), 021017 (Apr–Jun 2019), special ed. on The *Lynx* X-ray Observatory, 2019.

[2] [Bandler et al. 2016] S.R. Bandler et al., "Development of x-ray microcalorimeter imaging spectrometers for the X-ray Surveyor mission concept", Space Telescopes and Instrumentation 2016: Ultraviolet to Gamma Ray, edited by Jan-Willem A. den Herder, Tadayuki Takahashi, Marshall Bautz, Proc. of SPIE Vol. 9905, 99050Q 2016. doi: 10.1117/12.2232156.

[3] [Bennett et al. 2019] D. Bennett et al., "Microwave SQUID multiplexing for the *Lynx* X-ray microcalorimeter", Journal of Astronomical Telescopes, Instruments, and Systems 5(2), 021007 (Apr–Jun 2019), special ed. on The *Lynx* X-ray Observatory, 2019.

[4] [Devasia et al., 2019] A. Devasia et al., "Fabrication of Magnetic Calorimeter Arrays with Buried Wiring", IEEE Trans. Appl. Supercon. 99, 1-1, (2019) DOI: 10.1109/TASC.2019.2902530.

[5] [DiNigris et al., 2018] N. S. DeNigris, J. A.Chervenak, S.R Bandler, et.al., J. Low Temp Phys, 193, pp. 687-694 (2018). https://doi.org/10.1007/s10909-018-2019-8

[6] [DiPirro et al. 2019] M. DiPirro et al., "Lynx x-ray microcalorimeter cryogenic system", Journal of Astronomical Telescopes, Instruments, and Systems 5(2), 021006 (Apr–Jun 2019), special ed. on The *Lynx* X-ray Observatory, 2019.

[7] [Eckart et al. 2019] M.E. Eckart et al., "Design of optical/IR blocking filters for the Lynx X-ray Microcalorimeter", Journal of Astronomical Telescopes, Instruments, and Systems 5(2), 021020 (Apr–Jun 2019), special ed. on The *Lynx* X-ray Observatory, 2019.

[8] [Finkbeiner et al. 2015] F.M. Finkbeiner et al., "Development of Embedded Heatsinking Layers for Compact Arrays of X-Ray TES Microcalorimeters", IEEE Trans. Appl. Supercon. 21, pp. 223-226 (2011).

[9] [Irwin et al., 2010] K.D. Irwin et al., "Code-division multiplexing of superconducting transition-edge sensor arrays", Superconductor Science and Technology, Volume 23, 3, 034004 (2010). doi:10.1088/0953-2048/23/3/034004.

[10] [Jaeckel et al., 2019] F. T. Jaeckel et al., "Energy Calibration of High-Resolution X-Ray TES Microcalorimeters With 3 eV Optical Photons", IEEE Transactions on Applied Superconductivity (Volume: 29, Issue: 5, Aug. 2019).

[11] [Jhabvala et al., 2016] C.A. Jhabvala, D.J. Benford, R.P. Brekosky, et.al. J. Low Temp. Phys. 184, 615 (2016). https://doi.org/10.1007/s10909-016-1487-y

[12] [Lee et al. 2015] S.J. Lee et al., "Fine pitch transition-edge sensor X-ray microcalorimeters with sub-eV energy resolution at 1.5 keV", Appl. Phys. Lett. **107**, 223503 (2015); https://doi.org/10.1063/1.4936793.

[13] [Li et al., 2007] M.J. Li, T. Adachi, C.A. Allen, et. al. Proc. SPIE 6687, 668709 (2007). https://doi.org/10.1117/12.734152

[14] [Mates et al., 2017] J. Mates et al., "Simultaneous readout of 128 X-ray and gamma-ray

transition-edge microcalorimeters using microwave squid multiplexing," Appl. Phys. Lett. 111(6), 062601 (2017).

[15] [Morgan et al., 2016] K.M. Morgan et al., "Code-division-multiplexed readout of large arrays of TES microcalorimeters", Appl. Phys. Lett. 109, 112604 (2016); https://doi.org/10.1063/1.4962636.

[16] [Sakai et al. 2019] K. Sakai et al., "Development of space-flight compatible room temperature electronics for the Lynx x-ray microcalorimeter", Journal of Astronomical Telescopes, Instruments, and Systems 5(2), 021013 (Apr–Jun 2019), special ed. on The *Lynx* X-ray Observatory, 2019.

[17] [Smith et al. 2012] S.J. Smith et al., "Small Pitch Transition-Edge Sensors with Broadband High Spectral Resolution for Solar Physics", S.J. Smith, J.S. Adams, C.N. Bailey, S.R. Bandler, J.A. Chervenak, M.E. Eckart, F.M. Finkbeiner, R.L. Kelley, C.A. Kilbourne, F.S. Porter, J.E. Sadleir, Journal of Low Temperature Physics, Volume 167, Issue 3, pp 168175 (2012).

[18] [Smith et al. 2019] S.J. Smith et al., "Multi-absorber transition-edge sensors for X-ray astronomy", Journal of Astronomical Telescopes, Instruments, and Systems 5(2), 021008 (Apr–Jun 2019), special ed. on The *Lynx* X-ray Observatory, 2019.

[19] [Smith et al. 2019 (2)] S.J. Smith et al., "Towards 100,000-pixel microcalorimeter arrays using multi-absorber transition-edge sensors," submitted to the Journal of Low Temperature Physics, 2019, e-print available on arXiv.org at < https://arxiv.org/abs/1908.02687>.

[20] [Stevenson et al. 2019] T.R. Stevenson et al., "Magnetic calorimeter option for the *Lynx* X-ray Microcalorimeter", Journal of Astronomical Telescopes, Instruments, and Systems 5(2), 021009 (Apr–Jun 2019), special ed. on The *Lynx* X-ray Observatory, 2019.

[21] [Wassell et al. 2017] E. Wassell et al., "Fabrication of X-Ray Microcalorimeter Focal Planes Composed of Two Distinct Pixel Types", IEEE Trans. Appl. Supercon. 27, 2300205 (2011).

[22] [Yoon et al., 2018] W. Yoon et al., "Toward large field-of-view high-resolution X-ray imaging spectrometers: microwave multiplexed readout of 28 TES micro- calorimeters," J. Low Temp. Phys. 193, 258–266 (2018).